

PolInSAR Based Scattering Information Retrieval for Forest Aboveground Biomass Estimation

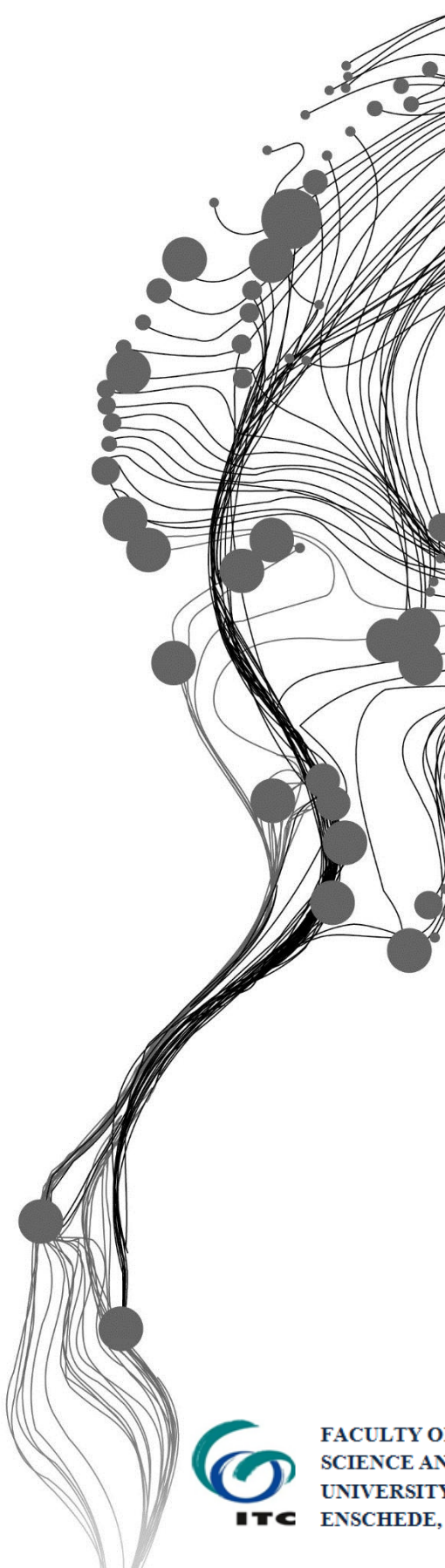
NEERAJ AGRAWAL

June, 2015

SUPERVISORS:

Mr. Shashi Kumar (IIRS)

Dr. Valentyn Tolpekin (ITC)



PolInSAR Based Scattering Information Retrieval for Forest Aboveground Biomass Estimation

NEERAJ AGRAWAL

Enschede, The Netherlands, [June, 2015]

Thesis submitted to the Faculty of Geo-Information Science and Earth Observation of the University of Twente in partial fulfilment of the requirements for the degree of Master of Science in Geo-information Science and Earth Observation.
Specialization: Geoinformatics

SUPERVISORS:

Mr. Shashi Kumar (IIRS)
Dr. Valentyn Tolpekin (ITC)

THESIS ASSESSMENT BOARD:

Chair	: Prof. Dr. Ir. M.G. Vosselman
ITC Professor	: Prof. Dr. Ir. A. Stein
External Examiner	: Mr. Sanjay (DEAL, Dehradun)
IIRS Supervisor	: Mr. Shashi Kumar
ITC Supervisor	: Dr. V. A. Tolpekin

OBSERVERS:

IIRS Observer	: Dr. SK Srivasatav
ITC Observer	: Dr. N.A.S. Hamm



FACULTY OF GEO-INFORMATION
SCIENCE AND EARTH OBSERVATION,
UNIVERSITY OF TWENTE,
ITC ENSCHEDE, THE NETHERLANDS



INDIAN INSTITUTE OF REMOTE SENSING
Indian Space Research Organisation
इसरो ISRO Department of Space, Government of India

DISCLAIMER

This document describes work undertaken as part of a programme of study at the Faculty of Geo-Information Science and Earth Observation of the University of Twente. All views and opinions expressed therein remain the sole responsibility of the author, and do not necessarily represent those of the Faculty.

DEDICATED TO MY LOVING
MOTHER AND FATHER

ABSTRACT

Forests play a crucial role in storing carbon and are of paramount importance in maintaining the global carbon cycle. Assessment of forest biomass at regional and global levels is vital for understanding and monitoring the health of both tree species and entire cover. The changes in forest biomass are caused as a consequence of human activities, natural factors and variations in climate. Thus, forest biomass quantification is necessary for gauging the changes in forest ecosystems. Hence, remote sensing techniques become indispensable for mapping forest biophysical parameters. Various remote sensing techniques are capable of collecting data even in cloud cover and at night as the microwaves are of long wavelength. Microwaves help in retrieving scattering information of target. The goal of this research was to map above ground biomass over Barkot forest range in Dehradun, India. The current work focuses on the retrieval of PolInSAR based scattering information for the estimation of above ground biomass. Radarsat-2 fully polarimetric C-band data was used for the estimation of AGB in Barkot forest area. A semi-empirical model which is an extended water cloud model (EWCM) was utilized for AGB estimation. Water cloud model (WCM) was not used because double bounce scattering or ground-stem interactions are not modelled in WCM. Extended water cloud model (EWCM) considers ground-stem interactions. EWCM considers some parameter, namely ground stem backscatter, ground backscatter, vegetation backscatter, total forest backscatter and empirically defined coefficient for the estimation of AGB. Due to overestimation of volume scattering polarization orientation angle shift was implemented on the PolInSAR pair. Field data was utilized for the accuracy assessment. The results show that coefficient of determination (R^2) value of 0.47, root mean square error (RMSE) of 56.18 ($t\ ha^{-1}$) and accuracy of 72% was obtained between modelled biomass against field biomass. Hence, it can be inferred from the obtained results that PolInSAR technique, in combination with semi-empirical modelling approach, can be implemented for estimating forest biomass.

Keywords: Extended water cloud model (EWCM), PolInSAR, biomass, backscatter, water cloud model (WCM), polarization orientation angle shift.

ACKNOWLEDGEMENTS

Foremost, I would like to thank my parents for their love, affection, belief and undying faith on my capabilities. Then I would like to thank my supervisor, Mr. Shashi Kumar Sir for motivating and encouraging me at every step. Without him I could not have completed my M.Sc. thesis. I would also like to thank my ITC supervisor, Dr. V.A. Tolpekin, for his great support and constantly correcting me in every aspect. I would like to express my deepest gratitude to Dr. Y.V.N. Krishna Murthy, Director IIRS, for providing all the opportunities and facilities that was required for the successful execution of the project. I am thankful to Dr. S.K. Srivastav and Mr. P.L.N. Raju sir for their valuable advices, and support during my research work.

I express my gratitude to my best friends Ankit, Shishant, Vikas, Mohit, Deepak. There are numerous unforgettable moments spent with them. They have supported me just like a brother. They have helped me in all the situations. I can never forget them.

I would like to thank my roommate Kiledar Singh Tomar for his constant love and caring nature. He has been a supporting factor in solving all biggest problems of my life. I would not have been able to complete this M.Sc. degree without his motivation and his friendship. He is not my friend but he is my brother. Next person to thank is Mr. Abhishek Saikia and Mr. Pratik Yadav. I will never forget ITC days in which my loving friend Abhishek Saaaakia cooked food for me as a gesture and my caring Pratik Yadav who made tea for me every day without losing a single day. I want Pratik to eat more and more food so that he becomes a bit healthy. All the memories with them in Euro trip is unforgettable. I enjoyed each and every moment with them.

I express my hearty gratitude to my seniors Deepak Chaudhary, Abhishek Sobhana, Kanishk Chaturvedi, Ishaan Kochhar, Unmesh Khati, Raj Bhagat, Guru Pradhan, Arvind Hari, Ponraj, Shashi Gaurav and Rohit Kumar for their moral support during my stay at IIRS. I also thank my M.Sc. friends Saikia, Pratik, Akshara, Vanya and Pranay for their love and support during ITC and IIRS stay. I would like to thank my M.Tech. batchmates Kavisha, Sanjay, Pratiman, Richa, Surya, Ram, Raja, Rohit, Vikrant, Joyson, Aniket, Vineet, Abhishek Das, Panini Das, Paaji, rajkumar, sukant, amol, kuldeep, Akshat, varun ,rigved. I am thankful to my PG Diploma friends Jagga, Sameep, Minakshi, Sanjeev, Saifu, Boka, Chauksi, Sambhu Sir and Amit Sir. I thank my GID trainees Jayant, Manish, Neetu, Sachin, Safreen and Joyson. My old and loving school friends and Btech. friends Shishant, Vikas, Mohit, Deepak, Ashu Yadav, Harsh, Gajendra, Manish, Nitesh, Sandeep, Miniraj, Prashant Chaturvedi, Indresh. I also extend my salutations to my beloved brothers and sisters for their understanding and love throughout my life. I also thanks my cma department hemant, ashish, ajay, Prakash, Rahul, awedwsh and azam.

TABLE OF CONTENTS

LIST OF FIGURES	v
LIST OF TABLES	vii
1. INTRODUCTION	1
1.1. MOTIVATION AND PROBLEM STATEMENT.....	3
1.2. RESEARCH IDENTIFICATION.....	4
1.2.1. RESEARCH OBJECTIVE.....	4
1.2.2. SUB-OBJECTIVE.....	4
1.2.3. RESEARCH QUESTIONS.....	4
1.3. INNOVATION AIMED AT.....	4
2. LITERATURE REVIEW	5
2.1. BIOMASS.....	5
2.2. RANDOM SAMPLING.....	6
2.3. RADAR REMOTE SENSING.....	7
2.4. POLARIZATION ELLIPSE.....	7
2.5. POLARIMETRIC SYNTHETIC APERTURE RADAR.....	9
2.6. POLINSAR (POLARIMETRIC SAR INTERFEROMETRY).....	11
3. STUDY AREA	14
3.1. BACKGROUND OF BARKOT FOREST.....	14
3.2. IMPORTANCE OF BARKOT FOREAT AREA.....	14
3.3. SOILS.....	14
3.4. MICROCLIMATE.....	14
3.5. FLORA.....	15
3.6. FAUNA.....	15
4. DATA MATERIAL AND METHODOLOGY	17
4.1. MATERIALS.....	17
4.1.1. SATELLITE DATA DESCRIPTION.....	17
4.1.2. FIELD SURVEY (BARKOT FOREST).....	17
4.2. METHODOLOGY.....	19
4.2.1. POLINSAR DATA PROCESSING.....	20
5. MODELLING APPROACH: WATER CLOUD MODEL (WCM) AND EXTENDED WATER CLOUD MODEL (EWCM)	29
5.1. WATER CLOUD MODEL.....	29
5.2. EXTENDED WATER CLOUD MODEL.....	31
6. RESULTS AND DISCUSSION	33
6.1. RELATION BETWEEN FIELD ESTIMATED AGB AND VOLUME SCATTERING RETRIEVEL FROM SAR IMAGES.....	33
6.2. SAR IMAGES (GRAY IMAGE).....	35
6.3. SURFACE AND DOUBLE BOUNCE SCATTERING OF POLINSAR IMAGE.....	35
6.4. POLINSAR VOLUME SCATTERING (BEFORE AND AFTER DE-ORIENTATION).....	37
6.5. RELATION BETWEEN FIELD ESTIMATED AGB AND VOLUME SCATTERING OF POLINSAR DATA.....	38

6.6.	COMPARISON VALUE OF POLINSAR IMAGE BEFORE AND AFTER DE-ORIENTATION..	40
6.7.	RGB IMAGE OF POLINSAR IMAGE (BEFORE AND AFTER DE-ORIENTATION).....	40
6.8.	BIOMASS ESTIMATION FROM EWCM.....	42
7.	DISCUSSION.....	45
8.	CONCLUSIONS AND RECOMMENDATIONS.....	48
8.1.	CONCLUSION.....	48
8.2.	RECOMMENDATION.....	49
	LIST OF REFERENCES.....	50
	APPENDIX.....	55
	DECOMPOSITION IMAGE OF RADARSAT-2 DATA.....	55

LIST OF FIGURES

Figure 2-1: Polarisation ellipse of electric field vector	7
Figure 2-2: Scattering mechanism containing various elements.....	8
Figure 3-1: Study area: Barkot forest in Dehradun, India	16
Figure 4-1: Sample plot area.....	18
Figure 4-2: Sample plot location in Barkot forest area	18
Figure 4-3: The field area consisting Sal forest, dry mixed miscellaneous forest, Khair-Sissoo forest and moist mixed miscellaneous forest. Most of the points lie in the Sal area since 57 percent area is covered by Sal forest.....	18
Figure 4-4: Flow diagram of Methodology.....	19
Figure 4-5: Generation of Master and Slave Images.....	20
Figure 4-6: Co-registration processing of Master and Slave Images	21
Figure 4-7: Yamaguchi decomposition model	23
Figure 4-8: Surface scattering.....	24
Figure 4-9: Double bounce scattering	25
Figure 4-10: Volume scattering.....	26
Figure 4-11: Helix scattering.....	26
Figure 5-1: Backscatter of ground σ_{gr}^0 and backscatter of vegetation σ_{veg}^0	29
Figure 5-2: Ground stem backscatter (σ_{gs}^0) from the canopy gaps	32
Figure 5-3: Ground stem backscatter (σ_{gr}^0) through the canopy gaps	32
Figure 6-1: Linear regression between field biomass (x axis) and volume scattering (y axis) of master image for 49 locations of field plots (28th January 2014).....	33
Figure 6-2: Linear Regression between field biomass (x axis) and Volume scattering (y axis) of slave image for 49 locations of field plots (20th February 2014).....	34
Figure 6-3: Volume scattering for master image.....	35

Figure 6-4: Volume scattering for slave image.....	35
Figure 6-5: Surface scattering of PolInSAR image.....	36
Figure 6-6: Double bounce scattering of PolInSAR image	36
Figure 6-7: Surface scattering before and after-deorientation.....	36
Figure 6-8: Double-bounce scattering before and after deorientation	37
Figure 6-9: PolInSAR based Volume scattering (before de-orientation)	37
Figure 6-10: PolInSAR based Volume scattering (after de-orientation).....	37
Figure 6-11: Linear regression between field biomass (x axis) and Volume scattering (y axis) of PolInSAR image for 49 locations of field plots (before de-orientation)	38
Figure 6-12: Linear regression between field biomass (x axis) and Volume scattering (y axis) of PolInSAR image for 49 locations of field plots (after de-orientation).....	39
Figure 6-13: Volume scattering values before and after de-orientation of PolInSAR image	40
Figure 6-14: PolInSAR RGB image before deorientation.....	41
Figure 6-15: PolInSAR RGB image after deorientation.....	41
Figure 6-16: Volume scattering for master, slave and PolInSAR image for 49 locations of field plots.....	41
Figure 6-17: Co-relation between field AGB (x axis) and modelled AGB (y axis) for 49 plots	42
Figure 6-18: Linear regression between field biomass against modelled biomass for the 15 plots	43
Figure 6-19: Linear regression between modelled biomass (y axis) and field biomass (x axis) for the thirty four plots.	44
Figure A: Yamaguchi decomposition of master image.....	55
Figure B: Yamaguchi decomposition of slave image.....	55

LIST OF TABLES

Table 4-1: Information regarding Radarsat-2 dataset	17
Table 6-1: Estimated R^2 value between volume scattering and field biomass of SAR images	34
Table 6-2: Estimated R^2 value between volume scattering and field biomass for the PolInSAR image before and after de-orientation	39
Table 6-3: R^2 , RMSE and percent accuracy obtained for modelled AGB.....	44

1. INTRODUCTION

Forests are the most vital renewable resources which play a substantial role in the existence of humans and the ecosystem ((Food and Agriculture Organization of the United Nations, 2012). They cover about 33% of the total landmass and play a major role in balancing global carbon cycle by exchanging of carbon i.e. sink or source ((Food and Agriculture Organization of the United Nations, 2012). Forests help in preserving the delicate balance of the local ecosystem. Also, they reduce the damage caused by natural disasters such as floods and avalanches. Forests however, are under stress due to the changing temperature and precipitation patterns. As such, constant monitoring of the exact amount of these resources have to be maintained (Kirilenko and Sedjo, 2007).

Biomass is an important parameter in evaluating the health of forests (Main-Knorn et al., 2011). Biomass of forest includes the sum of biomass which is above ground and below ground (Food and Agriculture Organization of the United Nations, 2004). Biomass estimation of forest through conventional (in-situ) method is a difficult and time consuming task. Researchers have developed remote sensing based modelling approaches for AGB estimation. Mainly three regions of the whole electromagnetic (EM) spectrum are being used in remote sensing for forest mapping and monitoring and these regions are visible region, thermal region and microwave region of EM spectrum. Optical remote sensing technique includes visible and near infrared region of EM spectrum and are widely used for retrieving the forest parameters. Wavelengths in the range of 1mm to 1m of electromagnetic spectrum are used for SAR remote sensing and the wavelengths of radar waves are very large in comparison to visible range.

Synthetic aperture radar (SAR) sensor transmits electromagnetic energy and receives the backscattered amount of energy after interaction with the objects on earth's surface. SAR sensor has an added advantage of forest canopy penetration and due to this penetration capability it is widely used for forest biophysical parameter retrieval.

Polarimetric Synthetic aperture radar (PolSAR) is an advanced remote sensing technique which has successfully proved its potential in modelling approaches for forest biophysical parameters retrieval (stem volume and biomass) (Amrutkar et al., 2012) (Wollersheim and Collins, 2008). In the current scenario, for the estimation of AGB of the forest area, researchers are using a combination of PolSAR decomposition and polarimetric SAR interferometry (PolInSAR). These techniques are better able to discriminate the backscattering from the objects lying in the same pixel leading to reliable scattering information for parameters retrieval.

SAR interferometry (InSAR) technique is concerned with investigating and consolidating the signs of the same object from varying angles and at distinctive times. Extraction of phase difference or common

interferogram by radar interferometry implies combination of coherent signals from two distinguished spatial positions (also known as baseline of interferometer). This is accomplished in radar by primarily two configurations i.e. along track interferometry and across track interferometry. Along track interferometry implies time displacement along the flight direction between distinguished antennas. While across track interferometry lead to spatial information by implying lateral separation between antennas which considers the scatterer elevation as a reference position. PolInSAR basically focuses on across track geometries but it can also be applied to along track geometries.

In the remote monitoring using airborne or satellite data, the vegetation parameters extraction like forest height (Hellmann and Cloude, 2005) and biomass (Mette et al., 2004), PolInSAR has vital applications. This technique combines two radar technologies such as SAR polarimetry and SAR interferometry. Polarimetry involves measuring the backscatter received from all four polarimetric combinations (HH, VV, VH and HV) (Cloude and Pottier, 1996). Using this, a 2×2 scattering matrix is retrieved which is then used to calculate image pixel (backscatter) value for any polarization combination (Cloude, 2008).

Decomposition modelling technique is used for retrieving the scattering elements. There are two types of decomposition modelling, namely, coherent decomposition and incoherent decomposition (Touzi et al., 2004) (Touzi, 2007). Coherent decomposition is able to characterize only the coherent targets which gives completely polarized backscatter, also known as point or pure scatterer (Touzi et al., 2004). Incoherent decomposition occurs in natural objects like in forest/vegetation areas which is characterised by coherency matrix. Three types of scattering mechanisms, namely, surface scattering, double bounce and volume scattering are explained by the Freeman-Durden decomposition model (Freeman and Durden, 1998). On the other hand, the Yamaguchi decomposition model (Yamaguchi et al., 2011) considers four scattering mechanisms, namely, surface, double-bounce, volume and helix scattering. Multiple component scattering models (Zhang et al., 2008) consider five scattering mechanisms, namely, surface, double-bounce, volume, helix and wire scattering.

PolSAR and PolInSAR based semi-empirical models have been used for forest ABG, stem volume and tree height estimation (Chowdhury et al., 2013) (Dinh et al., 2012). For AGB estimation, a very famous model water cloud model was developed by Attema et al., (Attema and Ulaby, 1978), which was further improved upon and used by several researchers. PolInSAR coherence based random volume over ground (RVoG) and interferometric water cloud model (IWCM) models were used for forest parameter retrieval using scattering elements (Papathanassiou and Cloude, 2001) (Cloude and Papathanassiou, 1998) (Santoro, 2003). In this study the concept of PolInSAR based scattering in semi-empirical modelling is utilised for AGB estimation.

1.1. MOTIVATION AND PROBLEM STATEMENT

Studies have been carried out to extract scattering information using fully polarimetric dataset for forest biophysical characterization (tree height, biomass, stem volume). Fully Polarimetric SAR data have shown its potential over single or dual polarimetric data in scattering information retrieval from single SAR resolution cell. Single SAR resolution cell contains multiple features. Possibility of more than one type of scattering elements is dependent on the diversification in the features within resolution cell. Use of single polarized or dual polarized SAR data does not provide the information of all the types of scatters available in the resolution cell. On the basis of interaction of electromagnetic wave with different type of objects, a number of approaches has been developed to retrieve all possible scattering elements from area (resolution cell) using PolSAR data (Jin and Feng, 2013). This work will utilize fully polarimetric SAR data with semi-empirical based model for the estimation of AGB of tropical forest.

Scattering information retrieved from SAR data of different dates do not show similar value for the same location. Coefficient of determination obtained from linear regression between volume scattering and AGB shows different values for the SAR dataset of different dates (Rahman and Sumantyo, 2013). Scattering information (Surface, double bounce and volume scattering) is an important input parameter for the modelling approaches used for AGB estimation. In this study an attempt was made to obtain reliable scattering information using a combination of two PolSAR images in interferometric mode.

Forest cover which behaves like volume scatterer does not keep the nature of definite scattering. The features which are responsible for volume scattering represents a chaotic scattering state because these are combination of several kinds of scattering from twigs, tree leaf i.e. all are contributing to volume scattering. It is expected that the combination of the two techniques i.e. PolSAR and PolInSAR would help in better discrimination of scatterers that lie in the same pixel.

In SAR backscatter, a saturation problem was noted by several researchers after a certain amount of AGB value (Imhoff, 1995). SAR backscatter technique after a certain volume of biomass reaches a saturation point after which it is unable to obtain more information about the biomass. Researchers found that saturation limit to estimate the biomass for forests was 100 tons/ha (0.44 GHz) for P-band, 40 tons/ha (1.25 GHz) for L-band and 20 tons/ha (5.3 GHz) for C-band (Imhoff, 1995). Whereas PolInSAR overcomes this saturation problem and helps to obtain the information which is difficult using the SAR backscatter technique.

The elevating importance of SAR remote sensing community for the retrieval of forest aboveground biomass makes both polarimetric SAR decomposition and polarimetric SAR interferometry a trending topic. Forest aboveground biomass has been successfully modelled using PolInSAR techniques in combination

with semi-empirical modelling and tree height has also been modelled using PolInSAR coherence estimation (Chandola, 2014). The current work focuses on the retrieval of reliable scattering information using PolInSAR based coherency matrix and retrieval of aboveground biomass using semi empirical model.

1.2. RESEARCH IDENTIFICATION

1.2.1. RESEARCH OBJECTIVE

To explore the potential of PolInSAR based scattering retrieval for semi-empirical modelling of forest aboveground biomass.

1.2.2. SUB-OBJECTIVES

- To retrieve PolInSAR coherency matrix elements for decomposition modelling.
- To evaluate the potential of PolInSAR based decomposition modeling for scattering information retrieval.
- To retrieve the semi-empirical model parameter for AGB estimation.
- To test the potential of modelling approach for AGB estimation.

1.2.3. RESEARCH QUESTIONS

- How to generate PolInSAR based coherency matrix elements for decomposition?
- How to evaluate the potential of PolInSAR based decomposition modelling for scatterings information retrieval?
- What parameters are required to model forest AGB?
- How can PolInSAR based modeling be used to estimate AGB?
- What is the accuracy of PolInSAR based semi empirical model for the modeled AGB using field data?

1.3. INNOVATION AIMED AT

Fully Polarimetric SAR data is used for scattering information retrieval from single SAR resolution cell. Single SAR resolution cell may contain contributions from more than one scattering objects. Hence, single or dual polarised data does not provide all the possible scattering information. So, to overcome this problem fully polarimetric data is used. Fully polarimetric data of different dates provide different scattering values for same object. Scattering values are important input elements for modelling of forest aboveground biomass. In this research work an approach is proposed to get reliable scattering from PolSAR data using interferometric pair. Innovation is aimed at modelling of AGB in a tropical forest using PolInSAR based scattering information.

2. LITERATURE REVIEW

2.1. BIOMASS

Forests covers 30% of the earth's physical surface (FAO, 2012). They are regular assets in carbon stockpiling through their connections with environment and soil (FAO, 2012). There is an expanding necessity for forest monitoring with respect to the climate change problem. For climate change carbon sequestration forms a vital part as forest act as carbon sink. This is done using biomass modelling. The imbalance in carbon stocks occurs because of land use change. Forest AGB biomass is a crucial quantity and remote sensing plays an important role for biomass mapping in less time. Forest biomass is the best integrative forest factor, and in conjunction with species organization it forms the key parameter in biodiversity. Total AGB includes biomass of individual structural parts of the tree including branches, tree leaf biomass and biomass of the stem (FAO, 2012) (Brown, 1997). Mette et al., (Mette et al., 2002) used polarimetric SAR interferometry for forest AGB estimation wherein forest height was identified as key parameter for forest AGB measurement and an allometric equation was developed between forest height and AGB using PolInSAR technique (Mette et al., 2004). There are four methods for estimating biomass:

- Harvest sampling technique or destructive sampling
- Non-destructive sampling
- Airborne/space borne remote sensing data
- Estimating biomass through modeling

Harvest sampling technique isolates the vegetation into different segments like extensions, twigs, leaves and stems. The crisp weight and the broiler dried weight of these parts are measured and biomass is estimated (Husch et al., 2003).

The vegetation components below forest canopy also contribute towards forest biomass and these are known as understory. The most widely recognized method to understory biomass determination is to anticipate biomass from non-destructive measurements of the plant. Low biomass is contributed by the bushes (understory) lying below forest canopy. This work mainly focuses on AGB contributed by forest trees. Non-destructive sampling is useful to find the area that is largely heterogeneous in vegetation. Various regression models have been created to anticipate biomass. The most well-known equation are (Husch et al., 2003).

$$A = d_0 + d_1 t \quad \text{Linear equation} \quad 2.1$$

$$A = d_0 + d_1 t + d_2 t^2 \quad \text{Quadratic equation} \quad 2.2$$

$$A = d_0 e^{d_1 t} \quad \text{Exponential equation} \quad 2.3$$

$$A = d_0 t^{d_1} \quad \text{Allometric equation} \quad 2.4$$

$$\log A = d_0 + d_1 \log t \quad \text{Logarithmic equation} \quad 2.5$$

where, A is biomass, d is regression coefficient and it is non-destructive plant measure. The equations from 2.1 to 2.5 are regression equations that uses stem breadth at the ground, stem diameter, crown area, plant height or grouping of these variables.

Several models are used for the biomass estimation such as empirical models and semi-empirical models. The empirical models works only with the field data and do not take into account the mathematical basis, whereas the semi empirical models operates with both field data as well as mathematical basis. Previous researchers (Lin and Sarabandi, 1998) (Haripriya, 2002) (Zianis et al., 2005) used empirical models for the derivation of biomass.

2.2. RANDOM SAMPLING

Sampling is a technique of selecting plots in the forest characterising the whole forest and is requires to derive parameters of the models. It is used as field data collection for validation. A sampling unit is selected in such a way that the other possible unit having the chances of being chosen will be equal. There are many types of sampling techniques. Stratified random sampling was used in the current study. This type of sampling unit is known as random sampling, where a table of random numbers is used to select a sampling unit from a well shuffled pack. Forest inventory uses the following random sampling techniques (Chaturvedi and Khanna, 1994).

- Simple random sampling
- Stratified random sampling
- Multistage sampling
- Multi-phase sampling
- Sampling with varying probability
- List sampling

Forest contains heterogeneous species of trees, which is subdivided into different strata from which a sampling unit is selected in the proportion of their size. This method of selecting sampling unit is known as stratified sampling method (Ding et al., 1998). Generally stratified sampling method brings down a heterogeneous forest into homogeneous groups called strata. This homogeneous group, i.e. forming strata, is often done by species, site qualities, crop density etc. (Husch et al., 2003) (Chaturvedi and Khanna, 1994).

2.3. RADAR REMOTE SENSING

A critical property that separates the radar waves from the optical waves is the penetration capability. Optical data are also used to estimate the biomass, but the problem lies in the inability to penetrate the cloud cover and work at night whereas the microwave remote sensing is capable to collect data in cloud cover and at night because the wavelengths are longer (Henderson and Lewis, 1998). Microwave has also been used to retrieve scattering information of the target.

Previous researches have utilized diverse wavelength to estimation the biophysical attributes of diverse vegetation sorts (Mette et al., 2004) (Santoro et al., 2006) (Carreiras et al., 2013). The amounts of transmitted energy backscattered from the target are related by the radar equation and can also be determined (Woodhouse, 2006).

$$P_r = \frac{A^2 P_t \sigma}{4\pi \lambda^2 R^4} \quad 2.6$$

Where P_t is the transmitted power by radar, P_r is the received power by radar, σ is the scattering coefficient, λ is the wavelength radar, R is the distance from antenna to the target and A is receiving antenna.

2.4. POLARIZATION ELLIPSE

An electric field plane is composed of horizontal component and vertical component vector and these components are characterized by the relative phase between them and their amplitudes. The electric field vector follows elliptical pattern in space in the propagation direction, this pattern in general is known as polarization ellipse (Henderson and Lewis, 1998). Polarisation ellipse is shown in figure 2-1.

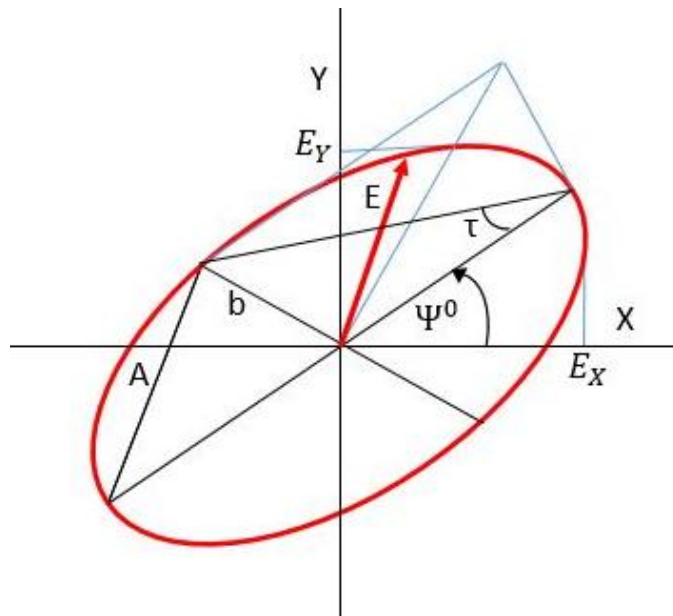


Figure 2-1: Polarisation ellipse of electric field vector

Polarization ellipse is characterized by polarization orientation angle and ellipticity. In figure 2-1, Ψ^0 is the orientation angle, E_x and E_y are the magnitude of X and Y component, b are semi major and minor axis, E resultant electric field vector is given equation 2.7.

$$E = \sqrt{E_x^2 + E_y^2} \quad 2.7$$

The shape of a polarization ellipse is given by three parameters,

- The amplitude of the ellipse, A , which is determined by the axis of the ellipse

$$A = \sqrt{E_x^2 + E_y^2} \quad 2.8$$

- The ellipse orientation is given by the angle between major and horizontal x axis. Where, Ψ^0 is ellipse orientation

$$\tan 2\Psi^0 = 2 \frac{E_x E_y}{E_x^2 - E_y^2} \cos \delta \quad \text{where } \delta = \delta_y - \delta_x \quad 2.9$$

- Ellipse aperture τ also known as ellipticity.

$$|\sin 2\tau| = 2 \frac{E_x E_y}{E_x^2 + E_y^2} |\sin \delta| \quad 2.10$$

Where, δ is a phase difference between E_x and E_y .

The orientation angle shift in built-up area is studied in a research work by Kimura (Kimura, 2008). The scattering from the built-up areas consists of three mechanisms i.e. single-bounce scattering from the roofs or roads, double-bounce scattering from wall and road and triple-bounce scattering from wall to next wall and then to road (as shown in figure 2-2). The POA is $\tan^{-1} \left(\frac{\tan \alpha}{\cos \phi} \right)$, where, α is wall and ϕ is the radar incidence angle.



a) Surface scattering

b) Double-bounce scattering

c) Triple bounce scattering

Figure 2-2: Scattering mechanism containing various elements

The orientation angle compensation affects the result of coherency matrix and decompositions such as Freeman-Durden and Yamaguchi decomposition. This effect was studied by Lee and Ainsworth (Lee and Ainsworth, 2011). It includes scattering elements such as volume scattering, double bounce, surface scattering and helix scattering. The power of volume scattering was reduced, for double-bounce scattering it increases and helix scattering power remains roll-invariant after shift in orientation angle. It was witnessed that the consequence of orientation angle compensation had an influence on 3×3 coherency matrix. After de-orientation process the real part of the element T_{23} became null. Intensity trend for HV and HH-VV became inversely related.

Iribe and Sato (Iribe and Sato, 2007), studied the dependence of POA shift on target structures especially the rotation angle of a particular structure. It was also found that orientation angle shift changed with the change in look direction of the radar. Using polarization orientation angle, rotation angle of the target could be easily estimated.

The orientation angle estimation procedures were discussed by Lee et al., (Lee et al., 2003). The estimation of polarisation angle is based on the circular polarisation. OA could be derived effectively using P-band data and L-band data whereas C-band data was less useful for the OA derivation.

2.5. POLARIMETRIC SYNTHETIC APERTURE RADAR

Polarimetry is a measurement and explanation of polarization state of electromagnetic waves. In SAR remote sensing polarimetric combinations are defined on the basis of the polarization state of transmitted and received signals. Cloude and Papathanassiou (Cloude and Papathanassiou, 1998) utilised the polarimetry for generation of coherent interferometry. The optimisation of coherence is performed in order to find out best scattering elements. The interferogram were generated which were independent of scattering elements. Chen et al., (Chen et al., 2012), explained a methodology to find out complex coherence. This complex coherence matrix follows Wishart distribution. Two types of information i.e. polarimetric information and interferometric information are used as a measure to search for homogeneous pixels in PolInSAR image. Maximum four polarimetric combinations are defined on the basis of horizontal and vertical polarization states and these are

HH – Horizontal transmit and Horizontal receive

HV - Horizontal transmit and Vertical receive

VH - Vertical transmit and Horizontal receive

VV - Vertical transmit and Vertical receive.

HV and VH are called cross polarized combination while HH and VV combination are called co-polarized. There are three levels of polarization.

Single polarized- HH or VV or HV or VH

Dual polarized- HH and HV, HH and VV, HV and VV

Quad polarized- HH, HV, VV, VH

Scattering matrix is a 2×2 matrix that describes polarization value derived using polarization combinations. Backscattered values retrieved from polarized SAR data for any location is influenced by wavelength of SAR system, orientation, surface roughness and moisture condition of objects lying in the particular location. Scattering matrix is given in equation 2.11.

$$S = \begin{bmatrix} S_{HH} & S_{HV} \\ S_{VH} & S_{VV} \end{bmatrix} \quad 2.11$$

The four elements obtained using scattering matrix are contained in every pixel. These elements can be retrieved from particular polarimetric combinations of SAR data. SAR systems work on two types of configurations: monostatic & bistatic. Monostatic systems have single antenna by which they transmit and receive signals while bistatic systems have separate antennas for transmitting and receiving signals (Lee and Pottier, 2009). According to assumption of reciprocity both the cross-polarized channels of monostatic SAR data carry similar information. After making this assumption only three polarimetric channels will be used in 2×2 scattering matrix (Woodhouse, 2006).

Coherent targets are only effective during scattering matrix analysis, whereas coherency or covariance matrix are effective for analysing complex targets (Touzi et al., 2004). Polarimetric parameters of complex targets can be retrieved using a 3×3 coherency matrix. It is the vectorised form of the scattering matrix S and its multiplication with the complex conjugate transpose is shown in equation 2.16 (Woodhouse, 2006). All nine parameter comprise physical information of the target. Coherency matrix and covariance matrix are represented as Pauli and Lexicographic basic. Lexicographic configures both the cross-polarized channels with the similar information. In the Lexicographic condition, covariance matrix C is given in equation 2.13.

$$K_L = \begin{bmatrix} S_{HH} \\ \sqrt{2}S_{HV} \\ S_{VV} \end{bmatrix} \quad 2.12$$

$$C = K_L \cdot K_L^T \quad 2.13$$

$$C = \begin{bmatrix} \langle |S_{HH} \cdot S_{HH}^*| \rangle & \sqrt{2} \langle S_{HH} \cdot S_{HV}^* \rangle & \langle S_{HH} \cdot S_{VV}^* \rangle \\ \sqrt{2} \langle S_{HV} \cdot S_{HH}^* \rangle & 2 \langle |S_{HV} \cdot S_{HV}^*| \rangle & \sqrt{2} \langle S_{HV} \cdot S_{VV}^* \rangle \\ \langle S_{VV} \cdot S_{HH}^* \rangle & \sqrt{2} \langle S_{VV} \cdot S_{HV}^* \rangle & \langle |S_{VV} \cdot S_{VV}^*| \rangle \end{bmatrix} \quad 2.14$$

In the Pauli condition, coherency matrix T is given in equation 2.16.

$$K_P = \frac{1}{\sqrt{2}} \begin{bmatrix} S_{HH} + S_{VV} \\ S_{HH} - S_{VV} \\ 2S_{HV} \end{bmatrix} \quad 2.15$$

$$T = \begin{bmatrix} \langle |S_{HH} + S_{VV}|^2 \rangle & \langle (S_{HH} + S_{VV})(S_{HH} - S_{VV})^T \rangle & 2 \langle (S_{HH} + S_{VV})S_{HV}^T \rangle \\ \langle (S_{HH} - S_{VV})(S_{HH} + S_{VV})^T \rangle & \langle |S_{HH} - S_{VV}|^2 \rangle & 2 \langle (S_{HH} - S_{VV})S_{HV}^T \rangle \\ 2 \langle S_{HV}(S_{HH} - S_{VV})^T \rangle & 2 \langle S_{HV}(S_{HH} + S_{VV})^T \rangle & 4 \langle |S_{HV}|^2 \rangle \end{bmatrix} \quad 2.16$$

For multilooking of the data scattering matrix is not averaged but the scattering matrix is converted into covariance/coherency matrix and then ensemble averaging ($\langle \rangle$) is performed.

2.6. POLINSAR (POLARIMETRIC SAR INTERFEROMETRY)

PolSAR and PolInSAR based semi-empirical models have been used for forest ABG, stem volume and tree height estimation (Chandola, 2014). For AGB estimation, a very famous model water cloud model was developed by Attema and Ulaby (Attema and Ulaby, 1978).

Water cloud model (WCM) based semi-empirical model

PolSAR decomposition based semi-empirical model for AGB estimation includes theoretical principal of WCM developed by Attema and Ulaby (Attema and Ulaby, 1978) and used by Santoro et al., (Santoro et al., 2006), Kumar et al., (Kumar et al., 2012). The semi-empirical model can be expressed in terms of scattering matrix element for surface and volume scattering. The Water Cloud Model relates forest parameters and forest backscatter. The assumptions considered by this model are that vegetation behaves like a homogeneous medium similar to a water droplet filled in a water cloud over a horizontal plane (Attema and Ulaby, 1978). This ground is modelled as plane and the forest scattering elements relate to water droplets in water cloud. Initially, some part of the incoming incident energy is reflected back to the sensor and the rest transmitted to the lower vegetation layer along with attenuation in terms of total forest backscatter.

$$\sigma_{total}^0 = e^{-\tau B} \sigma_{gr}^0 + (1 - e^{-\tau B}) \sigma_{veg}^0 \quad 2.17$$

where

σ_{total}^0 is total SAR backscatter

τ is empirically derived and is function of two way transmissivity

B is above ground biomass

σ_{gr}^0 is scattering from ground

σ_{veg}^0 is scattering from vegetation and it includes double-bounce and volume scattering

Extended water cloud model

Double bounce scattering because of the scattering from ground to stem of the tree should be considered for accurate biomass estimation which is not modelled in WCM (Poolla, 2013).

This the final equation of EWCM to find empirically defined coefficient (β) and AGB (B) (Poolla, 2013)

$$\sigma_{for}^0 = \sigma_{gr}^0 e^{-\beta B} + \sigma_{veg}^0 (1 - e^{-\beta B}) + \sigma_{gs}^0 e^{-\beta B} \quad 2.18$$

The forest height estimation using model-based inversion underestimated the forest height. Hence, Minh et al., (Minh et al., 2012) adopted a hybrid approach comprising of ESPIRIT method and coherence amplitude algorithm. This method proved to be efficient for forest height retrieval. PolInSAR data is used not only to derive forest height but also for estimation of height of buildings.

Mette et al., (Mette et al., 2004) retrieved biomass using PolInSAR data. For height derivation RVoG (random volume over ground) model was used. An allometric relationship between height and biomass was used to derive biomass. For dense forest results were quite good. For open forest due to the ground scattering this equation was not applicable. Hence, a modification in this equation was performed so as to include effective height of forest.

Ballester-Berman et al., (Ballester-Berman et al., 2005) modified the two layer inversion model for the agricultural crops. Earlier this inversion was used only for forest area. This method execute accurately when the value of coherence is above 0.3. This is applicable only to the vertical standing crops. This technique for dual polarized data (HH+VV, HH-VV) works better than the fully polarimetric data. Using this two layer model biophysical parameters were extracted. This was implemented for two crops like corn and rice crops. This was tested for various frequencies.

Lumsdon et al., (Lumsdon et al., 2008) used PolInSAR data i.e. ALOS PALSAR data for estimation of biomass. The study site for this was chosen as Kalimantan, Indonesia. Ground data was also collected for the purpose of validation. Tree height was extracted using random volume over ground (RVoG) model. The given framework was tested for both real satellite data as well as using simulated L-band data. The L-band data was simulated using PolSARPro. Under smooth conditions simulated data gave better results than the real satellite data.

Lavalle et al., (Lavalle et al., 2008) used PolInSAR data (L-band) for forest height estimation and other forest based parameters. Forest height was retrieved from coherent scattering model. PolInSAR scattering simulator PolSARProSim was utilised. Similar methodology was applied to compact polarimetric data.

Neumann et al., (Neumann et al., 2010) derived forest structure using multi-baseline PolInSAR data. It enhances the parameters retrieval separating the ground contributions. Cloude et al., (Cloude and Papathanassiou, 2003) used three stage inversion method for vegetation height estimation in such a way that there exist no variations due to topography. In previous study forest above ground biomass has been successfully modelled using PolInSAR techniques utilising semi-empirical model and tree height estimation using PolInSAR coherence (Chandola, 2014). The current work focuses on the retrieval of reliable scattering

information using PolInSAR coherency matrix based modelling approach and retrieval of aboveground biomass using semi empirical model. Parametric and non-parametric methods of regression were used for estimation of biomass by Neumann et al., (Neumann et al., 2011). L and P band airborne data was used. Two other methods that were used SVM (support vector machine) and random forest algorithm. The contributions from ground and also from the forest volume were separated. For L-band RMSE (root mean square error) of 28% and for P-band RMSE of 46% were obtained.

Lopez-Sanchez et al., (Lopez-Sanchez et al., 2012) used L-band airborne quad-pol data for estimation of height of crops such as rape, maize, wheat, barley and sugar beet. The PolInSAR data has been used earlier for forest not for crops. As L-band data is of low frequency hence, its penetration into the vegetation is high. Due to this the more backscatter occurs from the ground than from crop. To compensate for this phase to height sensitivity analysis was done for three baselines 30m, 60m and 90m. For height calculation RVoG (random volume over ground) model was used. This height obtained for rape and maize were nearly same as height from field data. But for wheat, barley and sugar beet this model overestimated the crop height.

Colin-Koeniguer and Trouvé (Colin-Koeniguer and Trouve, 2014) developed a framework for estimation of height of buildings. The study was conducted on high resolution SAR data of France. X-band data is utilized. This methodology has an advantage of removing layover effect which is a major problem in urban environment. Coherence optimization technique is used to remove the layover effect. ESPIRIT algorithm is used to derive interferometric phase of the scattering elements. Statistical analysis is performed for coherence shape of the buildings. This was tested for 140 buildings. Validation for the experiment was done using the ground truth data.

Le Toan et al., (Le Toan et al., 2014) discussed the challenges of using polarimetric (PolSAR) and interferometric (PolInSAR) data for biomass estimation. Two types of forests were addressed i.e. tropical and boreal forest. Biomass was retrieved for boreal forest and tropical forest using PolSAR dat. While, PolInSAR data was used for biomass estimation of both boreal and tropical forest. To improve the results combination of PolSAR and PolInSAR was used for biomass estimation.

A study for forest height and biomass estimation was performed by Huang et al., (Huang et al., 2014) using L-Band PolInSAR data. Boreal forest of Canada were chosen as study area. Validation was done using LiDAR data. Tomography was used to determine the forest structure. Allometric equation was used to estimate biomass. It was found that biomass estimation is dependent on forest height.

3. STUDY AREA

3.1. BACKGROUND OF BARKOT FOREST

In this research, the study area is Barkot forest, which lies between 28°43' N to 31°27' N (latitude) and 77°34' E to 81°02' E (longitude) in Uttarakhand state in the northern part of India. The study area situated in Shivalik range of Himalayas. The central part of the study area is Rajaji National Park, which is nearly mountainous with elevation ranging from 100 to 450 m. Study area contain tropical and subtropical moist broadleaf forest. Barkot forest is covered with grasses, shrubs, *shorea robusta* (Sal) and *Khair-sissoo* forest, *Tectona grandis* (Teak) and *Mallotus philippensis* (Rohini). This forest is gregarious in nature with mature Sal trees growing. In Dehradun district three types of Sal forest are found as dry shivalik Sal forest, moist Bhabar Doon, moist Shiwalik forest. The Area under study is 1800 km². Flora and fauna is the famous part of the Rajaji national part, which is situated of border of Barkot forest. The study area which is Barkot forest in Dehradun is depicted in figure 3-1.

3.2. IMPORTANCE OF BARKOT FOREAT AREA

This area suitable in this project because it provides all types of scattering as surface scattering, double-bounce scattering and volume scattering which are needed in this project. Study area is surrounded by agricultural area which provides ample volume scatterers through the growing period. The same area, without any vegetation growth provide surface scattering near the Barkot forest. This provides us with another opportunity to study the interaction of different scatterers of microwave. The terrain is relatively plain and hence the layover and shadow effect is not visible in the study area. Barkot forest very near to the organization so it is very easy to field data collection.

3.3. SOILS

Different type of soils as Alfisol, Molisol and Inceptisol are quite visible in this region. The soil which is fine Loamy Thermic Haplustalf occurs on the gentle sloppy terrain of the study area. The characteristic features of soils are absent because of abrupt change in texture and lithic contact up to 50 cm from the surface. These soils also have a characteristic argilic horizon and high base saturation status up to 1.25 m depth above the lithic contact. The soils are brownish in colour, acidic to near neutral in reaction and clay loam to silty loam in texture.

3.4. MICROCLIMATE

The climate state of the study zone is more calm and muggy than that of the boarding area. May and June are very blazing months. The temperature differs from 20°C (January) to 42°C (June) and during winter

season ice is common in this area, particularly from mid-December to mid-February, causing harm to Sal trees. Monsoon for the most parts starts before the end of June and rain proceeds until about the end of September. During July and August heavy rainfall happens, which represents 30.1% to 31.1% shower sometimes may fall in September and October. After that, there is normally little rain till before the end of December and some rain usually falls in January and December.

3.5. FLORA

Sal forest distributed three types of forest as mentioned in the paragraph 3.1. Mostly moist shiwalik forest are there in the Barkot forest and another two types Sal forest are present namely, moist shiwalik and moist Bhabar patches in souther slopes of the study area. All the tree species are there in the Barkot forest as mentioned in the paragraph 3.1. The forest is greatly affected due to growth of lantana weed because it is harmful of Barkot forest.

3.6. FAUNA

Barkot forest mainly contain elephants (*Elephas maximus*) which hence making survey by foot difficult also survey is risky due to presence of namely Neelgai (*Boselaphus tragocamelus*), Tigers (*Panthera tigris*), Samber (*Rusa unicolor*), Langoors (*Simia entellus*) and deer (*Axis axis*).

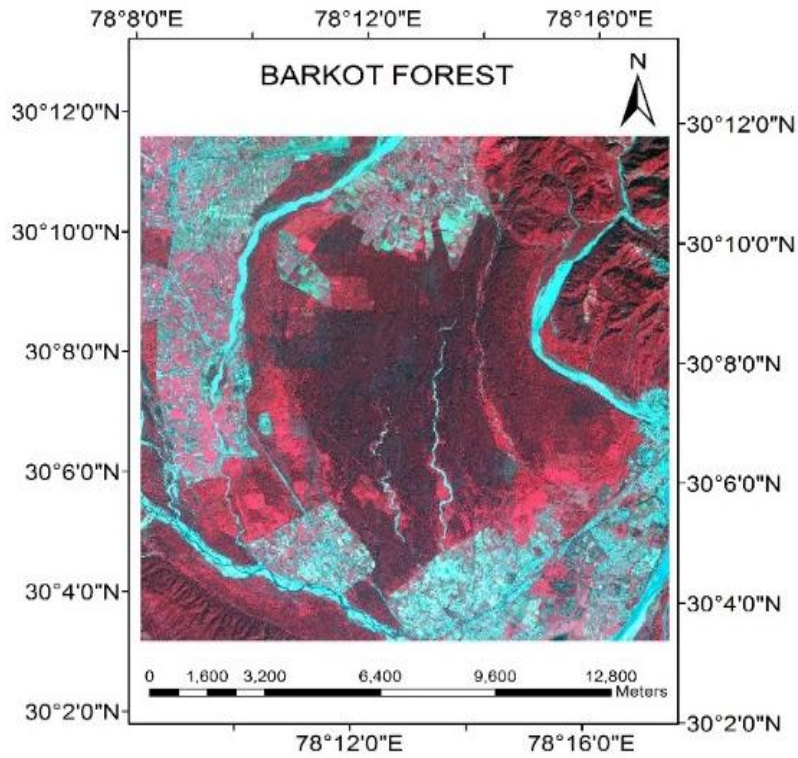
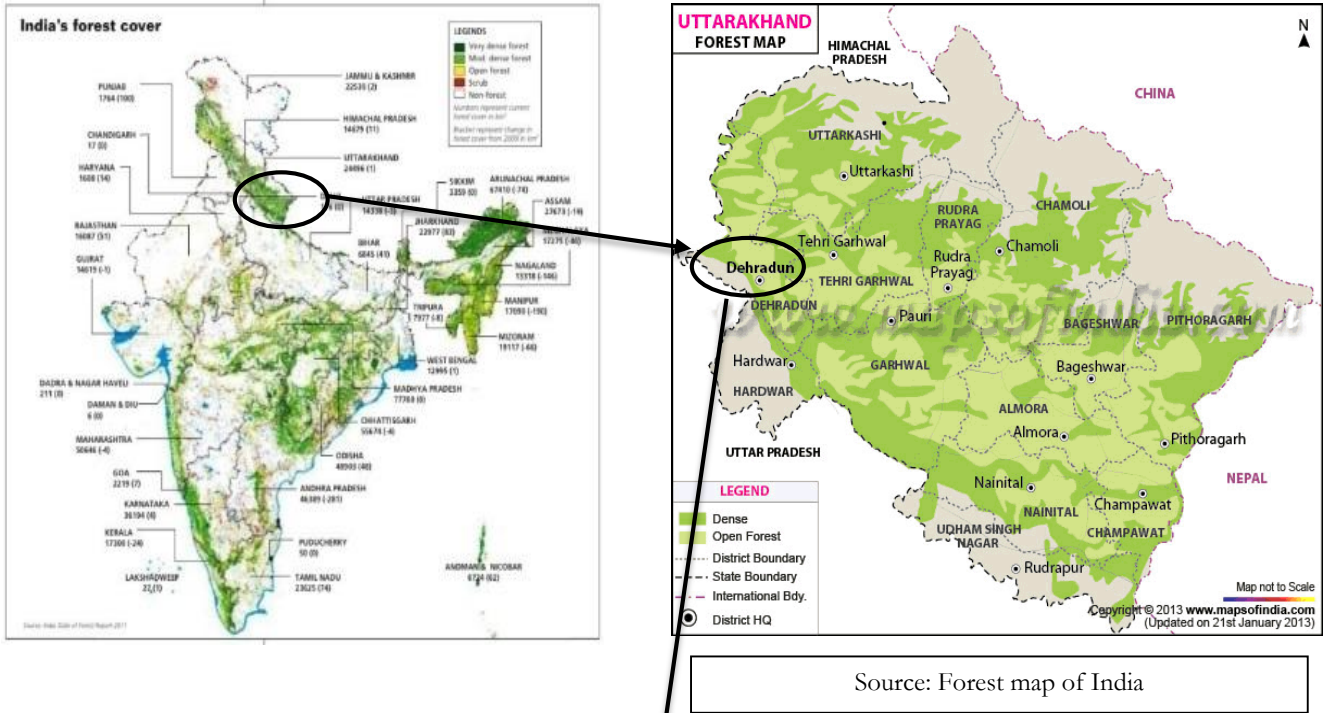


Figure 3-1: Study area: Barkot forest in Dehradun, India

4. DATA MATERIAL AND METHODOLOGY

4.1. MATERIALS

This chapter describes the satellite data utilized and the field work carried out for the PolInSAR data processing. The section 4.1.1 provides the description of Radarsat-2 satellite data utilized for the processing. The second section 4.1.2 describes the field survey of the Barkot forest area carried out to aid the processing. The section 4.2 illustrates the methodology devised for PolInSAR data processing to estimate AGB.

4.1.1. SATELLITE DATA DESCRIPTION

Single look complex (SLC) Radarsat-2 data is used in this study. Data acquired in fully polarized in C band data with wavelength 5.55 cm. Table 2 show that the all the information of Radarsat-2 data. This data was fully polarized based data and both the images were accessed with the gap of 23 days.

Source: Product files (Radarsat-2 data)

Table 4-1: Information regarding Radarsat-2 dataset

Date of acquisition	Beam	Incidence angle (far range)	Incidence angle (near range)
28 th January 2014 (Master image)	Q14	35.0°	33.4°
20 th February 2014 (Slave image)	Q14	35.0°	33.4°

4.1.2. FIELD SURVEY (BARKOT FOREST)

The field survey for data collection was carried out for Barkot forest during November 10th to December 5th, 2014. Forty nine sample plots were taken into observation for the research. Forty five sample plots data were already available and four more sample plots were chosen for the study. Stratified random sampling was used to collect field data for the measurement of circumference at breast height (CBH) ranged from 15 cm to 230 cm. These were later converted to diameter at breast height (DBH) for AGB calculation. Square plotting of 0.1 ha (31.62 m × 31.62 m) with square shaped sample plots were used. By the utilizing of DBH and tree height estimated the AGB. For the calculating AGB (as shown in equation 4.1) need to volumetric equation and specific gravity. So forest survey of India define the volumetric equation (Forest Survey of India, 1996) and Indian woods (Limaye and Sen, 1956) define the specific woods so it can be easily calculate AGB. FSI equation (stem volume equation and specific gravity volume) is mentioned for all the species. Four plots were calculated by the use of FSI equation and four plots show biomass 237.22 (t ha⁻¹), 264.59 (t ha⁻¹), 221.42 (t ha⁻¹) and 282.92 (t ha⁻¹). Positional errors of 6 m to 9 m were observed in GPS readings during the field data collection. Table 4-2 clearly defines which parameters measured and which methods were used for the tree height and CBH. Final AGB calculated ranged between 112.58 (t ha⁻¹) - 356.08 (t ha⁻¹). The details regarding field data are given in table 4-2 and various forest types in the plots are described in table 4-3.

AGB equation is given in equation 4.1 as follows.

$$AGB = \text{stem volume} \times \text{specific gravity} \quad 4.1$$

Table 4-2: Description of field data

PARAMETERS MEASURED	METHOD
Number of Sample Plots	49
Size of Sample Plots	31.62 m × 31.62 m
Shape of Sample Plots	Square
CBH	Measurement of circumference at breast height
Tree height	Measured using laser dendrometer

Table 4-3: Various forest types where Forty nine sample plots are collected

Forest type	Plots
Sal forest and Mix Sal forest	23
Teak plantation	9
Mix-Teak plantation	4
Acacia	2
Holoptelea plantation	5
Mixed forest	6

Source: Chandola 2013

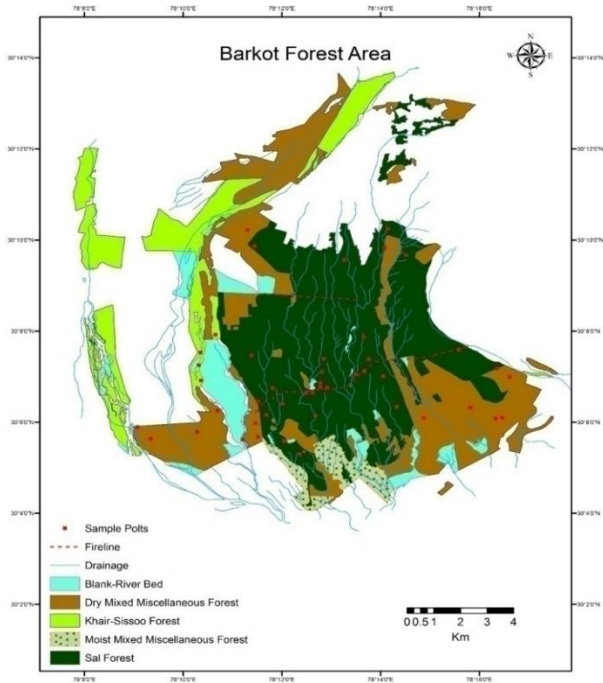


Figure 4-3: The field area consisting Sal forest, dry mixed miscellaneous forest, Khair-Sissoo forest and moist mixed miscellaneous forest. Most of the points lie in the Sal area since 57 percent area is covered by Sal forest.

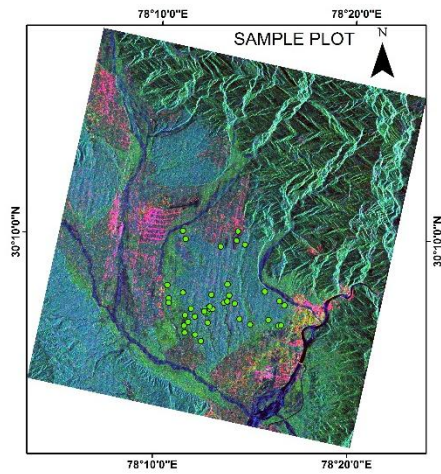


Figure 4-2: Sample plot location in Barkot forest area

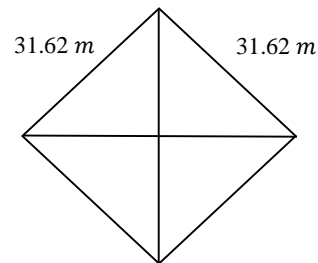


Figure 4-1: Sample plot area

Each plot of 31.62 m side

4.2. METHODOLOGY

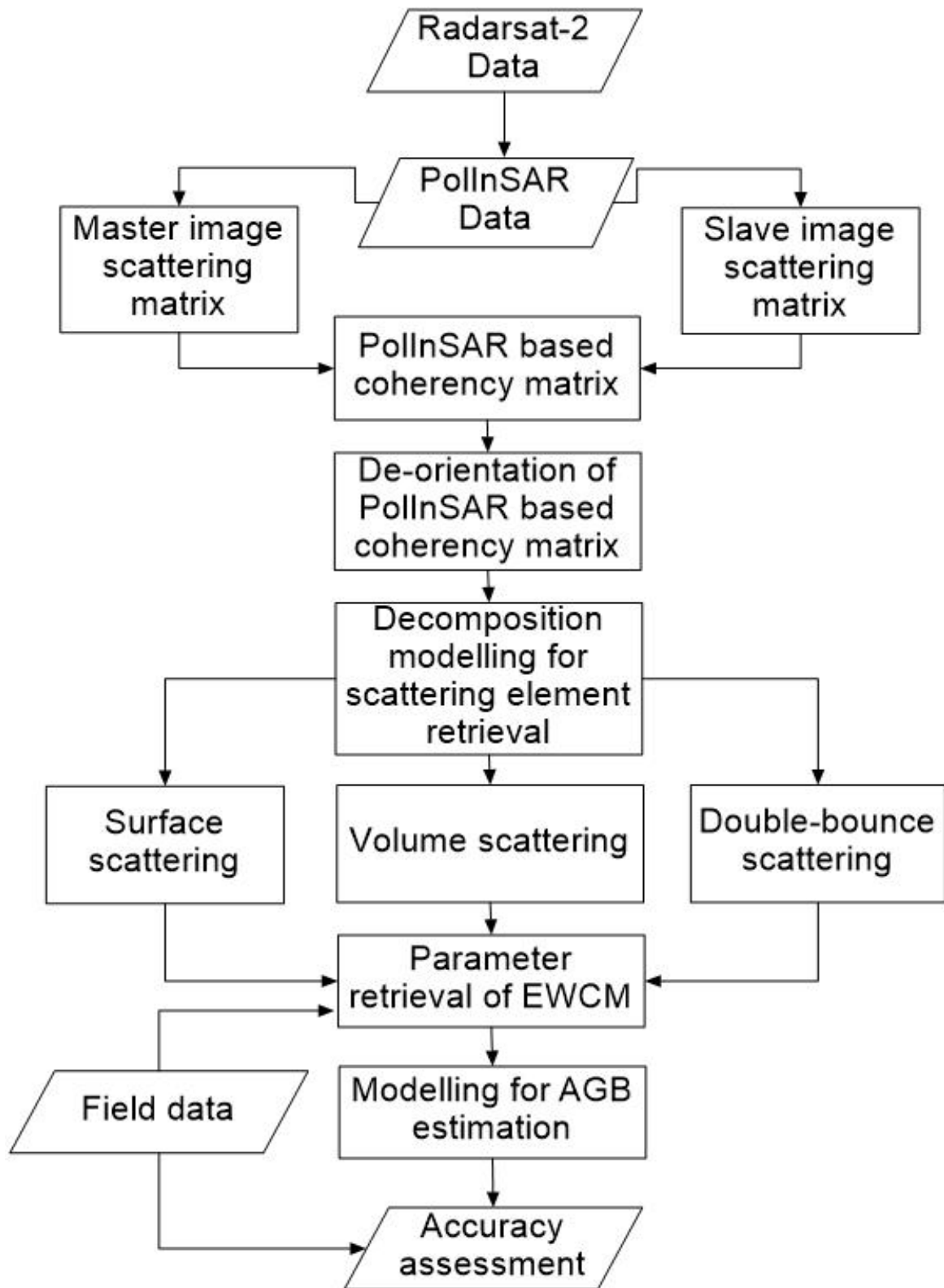


Figure 4-4: Flow diagram of Methodology

4.2.1. POLINSAR DATA PROCESSING

The PolInSAR data processing was carried out in few stages, which are defined further down. First of all scattering matrix was generated for both master and slave image. Co-registration was performed for SAR image pair. PolInSAR based coherency matrix was generated for the co-registered images. PolInSAR image was De-orientated and decomposition of de-orientated image was done. From decomposition three scattering elements i.e. surface scattering, volume scattering and double-bounce scattering were extracted. These parameters were given as input to EWCM model for estimating biomass. The field data and modelled biomass were compared to each other. Accuracy assessment was done using RMSE and percent accuracy.

- Generation of master and slave image scattering matrix
- Co registration of master and slave image
- PolInSAR based coherency matrix
- PolInSAR based decomposition of coherency matrix
- De orientation of PolInSAR based coherency matrix

4.2.1.1. GENERATION OF MASTER AND SLAVE IMAGE SCATTERING MATRIX

PolInSAR image was generated by using SAR images (Master image and slave image) using interferometry. Both images show relationship between polarimetric mode and interferometric mode. Master image is taken from January 28, 2014 and slave image is taken from February 20, 2014. Scattering matrix generated from Master and Slave images is given in equation 4.2 and 4.3 respectively. Both the images are taken from the same range for the diverse plots in two distinctive time periods. Table 4-1 illustrates all the information related to master and slave images.

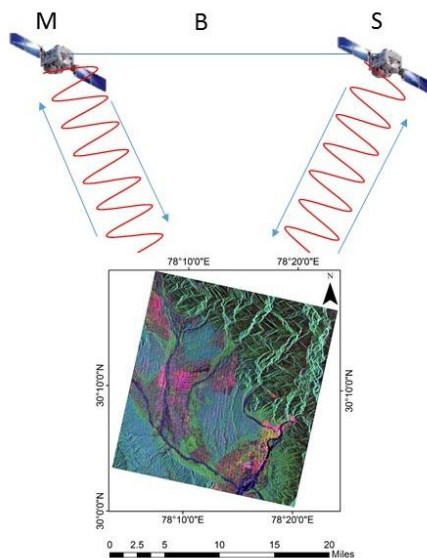


Figure 4-5: Generation of Master and Slave Images

$$[S_M] = \begin{bmatrix} S_{HH}^M & S_{HV}^M \\ S_{VH}^M & S_{VV}^M \end{bmatrix} \quad 4.2$$

$$[S_S] = \begin{bmatrix} S_{HH}^S & S_{HV}^S \\ S_{VH}^S & S_{VV}^S \end{bmatrix} \quad 4.3$$

where, M is a master image, S is a slave image and B is a baseline showing distance in the middle of two platforms.

4.2.1.2. CO-REGISTRATION OF MASTER AND SLAVE IMAGE

Image co-registration is significant part of PolInSAR data processing which is used for the alignment of two SAR images so as to get their phase difference. Co-registration is applied on SAR image pair (Li and Bethel, 2008). The Images provided as input for the co registration function are complex. SAR image pair used have same type (i.e. complex) and same projection system (all slant range or all ground range projected or all geocoded), otherwise the slave image(s) must be reprojected into the projection system of the master image. As the reference of master image, the slave image is co-registered and estimated for any shifts in the rows and columns of SAR image pair.

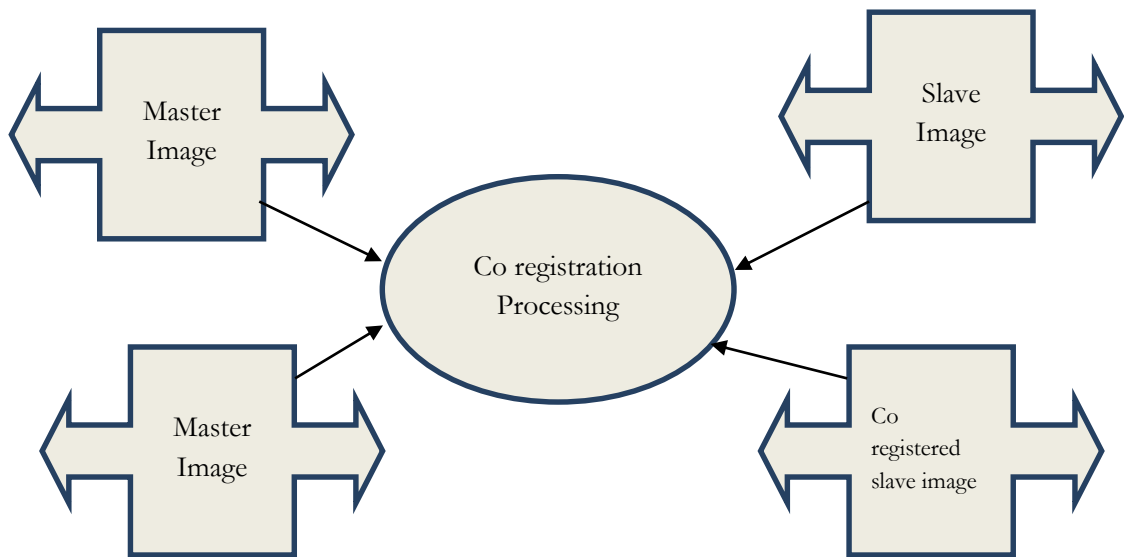


Figure 4-6: Co-registration processing of Master and Slave Images

4.2.1.3. POLINSAR BASED COHERENCY MATRIX

Berman and Sanchez (Berman and Sanchez, 2010) made an approach to generate 3×3 covariance matrix using PolInSAR pair of Radarsat-2 dataset. The covariance matrix was generated with the help of lexicographic matrixes obtained from PolInSAR pair and Freeman-Durden three component model was adopted to generate surface, double-bounce and volume scattering elements.

Previously all the decomposition model were developed using covariance matrix. After getting the sensitivity of POA (Lee and Ainsworth, 2011) of SAR data with coherency matrix element all the decomposition modelling are again redefined in terms of coherency matrix elements. An approach to get coherency matrix elements from PolInSAR pair was implemented to get scattering elements from coherency matrix based Yamaguchi four component decomposition model (Yamaguchi et al., 2011). The advantage of coherency matrix is revealed in a work of Yamaguchi.

PolInSAR based coherency matrix (T) was generated with the help of co-registered Master and Slave images. Pauli feature vector of master image K_M was multiplied with the transpose of complex conjugate of slave image K_S^{t*} (Berman and Sanchez, 2010). The decomposition of T was done using the four components Yamaguchi decomposition. All the components of the decomposition are Hermitian, and the T is not hermitian matrix as given in equation 4.7. Some assumptions were considered in the coherency matrix to justify this statement. The modulus of diagonal elements of the coherency matrix were taken to avoid the ambiguity of hermitian matrix property. According to the properties of hermitian matrix (Jahan and Ahmed, 2010) diagonal elements must be real and PolInSAR based coherency matrix diagonal elements are not real. To preserve the properties of PolInSAR based coherency matrix following assumption was made where modulus of diagonal elements of T were taken.

Off diagonal elements of lower triangular part of coherency matrix were assumed to be similar to the complex conjugate of the corresponding element in off diagonal element of upper triangular part of coherency matrix.

Coherency matrix based four component decomposition developed by Yamaguchi et al. (Yamaguchi et al., 2011) includes 6 elements ($T_{11}, T_{12}, T_{13}, T_{22}, T_{23}$ and T_{33}) of coherency matrix. The Same 6 elements were considered for four component decomposition using PolInSAR based coherency matrix. For future recommendation all the nine elements of coherency matrix can be used.

Since PolInSAR coherency matrix is not hermitian. Thus, to continue the process of decomposition, off-diagonal elements (T_{21}, T_{31}, T_{32}) were not used. In this modelling one assumption was made that the elements ($T_{12} = T_{21}^*$), ($T_{13} = T_{31}^*$) and ($T_{23} = T_{32}^*$). PolInSAR coherency matrix was generated by own procedure and the elements of generated matrix were used as an input in the software PolSAR pro for Yamaguchi four component decomposition. The decomposition method was adapted from Yamaguchi et al (Yamaguchi et al., 2011).

$$T = K_M \cdot K_S^{t*} \quad 4.4$$

$$K_M = \frac{1}{\sqrt{2}} \begin{bmatrix} S_{HH}^M + S_{VV}^M \\ S_{HH}^M - S_{VV}^M \\ 2S_{HV}^M \end{bmatrix} \quad 4.5$$

$$K_S^{t*} = \frac{1}{\sqrt{2}} [S_{HH}^S + S_{VV}^S S_{HH}^S - S_{VV}^S 2S_{HV}^S]^* \quad 4.6$$

$$T = \begin{bmatrix} \langle (S_{HH}^M + S_{VV}^M) \cdot (S_{HH}^S + S_{VV}^S) \rangle & \langle (S_{HH}^M + S_{VV}^M) \cdot (S_{HH}^S - S_{VV}^S) \rangle & 2 \langle (S_{HH}^M + S_{VV}^M) \cdot (S_{HV}^S) \rangle \\ \langle (S_{HH}^M - S_{VV}^M) \cdot (S_{HH}^S + S_{VV}^S) \rangle & \langle (S_{HH}^M - S_{VV}^M) \cdot (S_{HH}^S - S_{VV}^S) \rangle & 2 \langle (S_{HH}^M - S_{VV}^M) \cdot (S_{HV}^S) \rangle \\ 2 \langle (S_{HV}^M) \cdot (S_{HH}^S + S_{VV}^S) \rangle & 2 \langle (S_{HV}^M) \cdot (S_{HH}^S - S_{VV}^S) \rangle & 4 \langle (S_{HV}^M) \cdot (S_{HV}^S) \rangle \end{bmatrix} \quad 4.7$$

$$T = \begin{bmatrix} T_{11} & T_{12} & T_{13} \\ T_{21} & T_{22} & T_{23} \\ T_{31} & T_{32} & T_{33} \end{bmatrix}$$

where, T is Coherency matrix

After multiplying both the images (master and slave) coherency matrix was generated. To avoid the ambiguity of hermitian value of coherency matrix modules of diagonal elements are taken. Here, $\langle \rangle$ is ensemble average for SAR image pair, * is complex conjugate.

4.2.1.4. POLSAR BASED DECOMPOSITION OF COHERENCY MATRIX

Decomposition modelling is used for retrieving the scattering elements from coherency matrix. Huyen (Huynen, 1970) first used the target decomposition technique. Cloude and Pottier (Cloude and Pottier, 1996) reviewed the potential of different decomposition modelling approaches for scattering information retrieval from PolSAR data. There are two types of decomposition modelling, coherent decomposition and incoherent decomposition. Three types of scattering mechanisms; surface scattering, double bounce and volume scattering were deliberated by the Freeman-Durden decomposition model (Freeman and Durden, 1998). The Yamaguchi decomposition model (Yamaguchi et al., 2011) considers four scattering mechanism surface, double-bounce, volume and helix scattering (shown in Figure 4-7).

Source: Yamaguchi et al. 2011

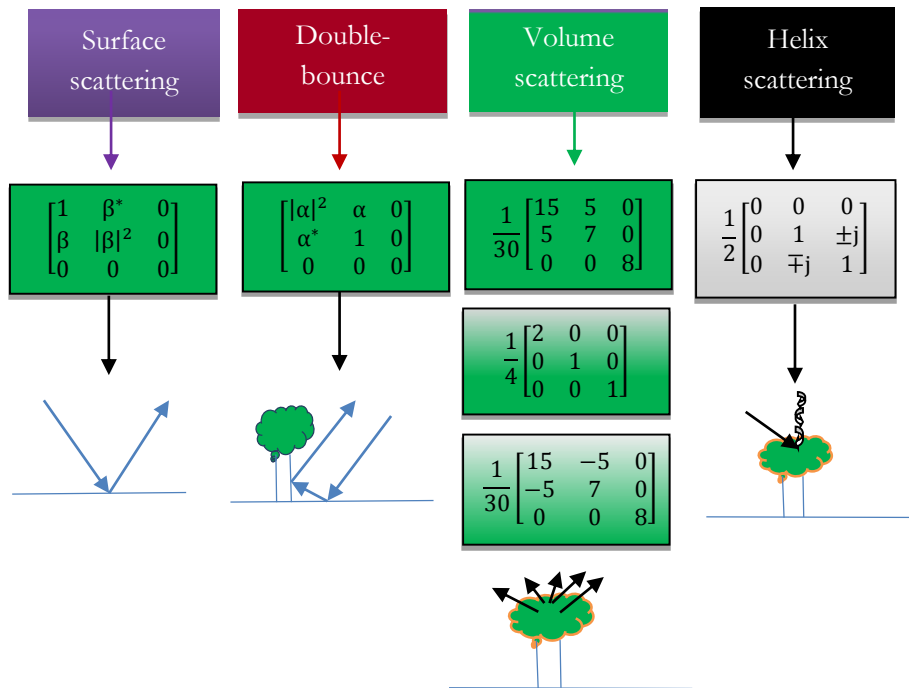


Figure 4-7: Yamaguchi decomposition model

The Multiple Component Scattering Model (Zhang et al., 2008) considers five scattering mechanism surface, double-bounce, volume, helix and wire scattering. Yamaguchi decomposition model:

$$T = P_s T_s + P_d T_d + P_v T_v + P_h T_h \quad 4.8$$

where, P_s , P_d , P_v , P_h are power for surface, double-bounce, volume, helix scattering and T_s , T_d , T_v , T_h are the expansion matrix for surface, double-bounce, volume, helix scattering.

The Yamaguchi uses four-component scattering matrix for the decomposition of the coherency matrix into four matrix relating to different scattering component.

Surface scattering- To represent this type of scattering mechanism a similar scattering matrix is used. This matrix represents odd bounce scattering. Odd bounce scattering consists of single and triple bounce scattering. Single-bounce scattering occurs from the roofs and streets. The surface scattering is represented in the form of coherency matrix (Yamaguchi et al., 2011). It is depicted in figure 4-8.



Figure 4-8: Surface scattering

$$f_s[T]_s = \begin{bmatrix} 1 & \beta^* & 0 \\ \beta & |\beta|^2 & 0 \\ 0 & 0 & 0 \end{bmatrix} \quad 4.9$$

$$\beta = \frac{R_H - R_V}{R_H + R_V} \quad 4.10$$

where, R_H and R_V are the Fresnel reflection coefficients for vertically and horizontally polarized wave.

Double bounce scattering- This sort of scattering is shown by ground-tree backscatters. The coherency matrix for double bounce scattering is given by (Yamaguchi et al., 2011). This type of scattering is shown in figure 4-9.

$$[T]_d = \begin{bmatrix} |\alpha|^2 & \alpha & 0 \\ \alpha^* & 1 & 0 \\ 0 & 0 & 0 \end{bmatrix} \quad 4.11$$

$$\alpha = \frac{e^{2j\gamma_H} R_{TH} R_{GH} + e^{2j\gamma_V} R_{TV} R_{GV}}{e^{2j\gamma_H} R_{TH} R_{GH} - e^{2j\gamma_V} R_{TV} R_{GV}} \quad 4.12$$

where, R_{GH} and R_{TH} is Reflection coefficients of the ground and tree (horizontal polarization).

R_{GV} and R_{TV} is Reflection coefficients of the ground and tree (vertical polarization). $e^{2j\gamma_H}$ and $e^{2j\gamma_V}$ is Propagation factors.



Figure 4-9: Double bounce scattering

Volume scattering- Volume scattering explains different scattering happening due to vegetation. This scattering is demonstrated by considering the vegetation cover as a cylinder. The coherency matrix for volume scattering is given by (Yamaguchi et al., 2011). It is shown in figure 4-10.

$$[T]_v = \begin{bmatrix} 2 & 0 & 0 \\ 0 & 1 & 0 \\ 0 & 0 & 0 \end{bmatrix} \quad 4.13$$

f_v is Expansion coefficients of volume scattering.

Yamaguchi modified the volume scattering and the three equations are defined as follows

$$[T]_v = \frac{f_v}{30} \begin{bmatrix} 15 & 5 & 0 \\ 5 & 7 & 0 \\ 0 & 0 & 8 \end{bmatrix} \quad 4.14$$

$$\text{For } 10 \log(\langle |S_{VV}|^2 \rangle / \langle |S_{HH}|^2 \rangle) < -2dB \quad 4.15$$

$$[T]_v = \frac{f_v}{4} \begin{bmatrix} 2 & 0 & 0 \\ 0 & 1 & 0 \\ 0 & 0 & 1 \end{bmatrix} \quad 4.16$$

$$\text{For } 10 \log(\langle |S_{VV}|^2 \rangle / \langle |S_{HH}|^2 \rangle) < 2dB \quad 4.17$$

$$[T]_v = \frac{f_v}{30} \begin{bmatrix} 15 & -5 & 0 \\ -5 & 7 & 0 \\ 0 & 0 & 8 \end{bmatrix} \quad 4.18$$

$$\text{For } 10 \log(\langle |S_{VV}|^2 \rangle / \langle |S_{HH}|^2 \rangle) > 2 \text{ dB} \quad 4.19$$



Figure 4-10: Volume scattering

Helix scattering- This sort of scattering can be seen from the complex structures and targets. A whole circularly polarized wave is produced from four dipoles arranged at an edge of 45° with a dividing of $\lambda/8$ wavelength or using dihedral corner reflectors arranged at 45° with $\lambda/4$ wavelength. The coherency matrix for helix scattering is given by (Yamaguchi et al., 2011). It is shown in figure 4-11.

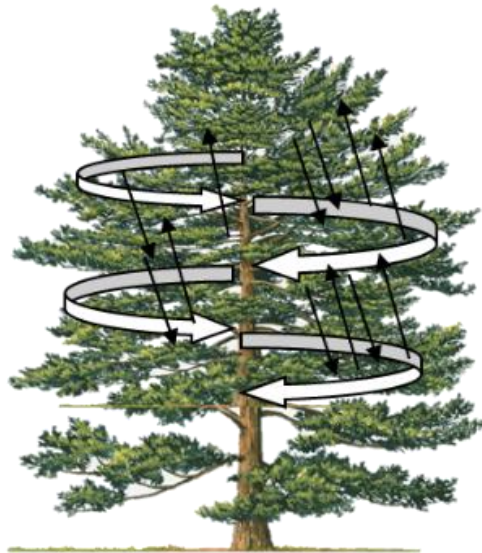


Figure 4-11: Helix scattering

$$f_s[T]_h = \frac{1}{2} \begin{bmatrix} 0 & 0 & 0 \\ 0 & 1 & \pm j \\ 0 & \mp j & 1 \end{bmatrix} \quad 4.20$$

The coherency matrix however, was combined into its corresponding scattering elements as given in equation 4.21.

$$T = f_s[T]_s + f_d[T]_d + f_v[T]_v + f_h[T]_h \quad 4.21$$

$$T = f_s \begin{bmatrix} 1 & \beta^* & 0 \\ \beta & |\beta|^2 & 0 \\ 0 & 0 & 0 \end{bmatrix} + f_d \begin{bmatrix} |\alpha|^2 & \alpha & 0 \\ \alpha^* & 1 & 0 \\ 0 & 0 & 0 \end{bmatrix} + f_v \begin{bmatrix} 2 & 0 & 0 \\ 0 & 1 & 0 \\ 0 & 0 & 0 \end{bmatrix} + \frac{f_h}{2} \begin{bmatrix} 0 & 0 & 0 \\ 0 & 1 & \pm j \\ 0 & \mp j & 1 \end{bmatrix} \quad 4.22$$

where f_s, f_d, f_v and f_h are the expansion coefficients of surface, double, volume and helix scattering. All the terms are shown in the form of scattering elements as stated below:

$$f_h = 2|\text{Im}\langle S_{HV}^*(S_{HH} - S_{VV}) \rangle|$$

$$f_v = 8\langle |S_{HV}|^2 \rangle - 4|\text{Im}\langle S_{HV}^*(S_{HH} - S_{VV}) \rangle|$$

$$f_s = B, f_d = A, \alpha = \frac{C}{A}, \beta^* = \frac{C}{B}$$

$$\text{Where } A = \frac{1}{2} \langle |S_{HH} - S_{VV}|^2 \rangle - 2\langle |S_{HV}|^2 \rangle$$

$$B = \frac{1}{2} \langle \langle |S_{HH} + S_{VV}|^2 \rangle - 4\langle |S_{HV}|^2 \rangle + 2|\text{Im}\langle S_{HV}^*(S_{HH} - S_{VV}) \rangle| \rangle$$

$$A = \frac{1}{2} \langle (S_{HH} + S_{VV})(S_{HH} - S_{VV})^* \rangle$$

Total scattering power is given in equation 4.23. The power matrix can also be represented in terms of expansion coefficients as given below.

$$\text{Total scattering power is } P_s + P_d + P_v + P_h \quad 4.23$$

$$\text{where } P_s = f_s(1 + |\beta|^2)$$

$$P_d = f_d(1 + |\alpha|^2)$$

$$P_v = f_v$$

$$P_h = f_h$$

4.2.1.5. DE-ORIENTATION OF POLINSAR BASED COHERENCY MATRIX

POA is an angle between the semi-major axis of polarization ellipse and direction of propagation of electromagnetic wave (as shown in figure 2-1) which gets changed after interaction with objects. The shift in POA may occur due to the shape and orientation of the object. Overestimation of volume scattering and

underestimation of double-bounce scattering was observed due to POA shift. POA compensation of SAR data is recommended to minimize the overestimation and underestimation problem. The POA shift compensation implemented on both the data of PolInSAR pair. Using POA compensated data 3×3 coherency matrix will be generated as shown in equation 4.7 (Woodhouse, 2006). Finally decomposition modelling of generated coherency matrix will provide surface, double-bounce and volume scattering. It uses the coherency matrix to define the scattering behaviour of forest. Lee et al., (Lee et al., 1999) characterize a method focused on the circular polarization. For the estimation of the orientation angle from the PolSAR data. The following formula is used for the estimated OA shift (ρ).

$$\rho = \begin{cases} \theta, & \text{if } \theta \leq \frac{\pi}{4} \\ \theta - \frac{\pi}{4}, & \text{if } \theta > \frac{\pi}{4} \end{cases}$$

$$\theta = \frac{1}{4} \left[\tan^{-1} \left(\frac{-4\text{Re}(\langle (S_{HH} - S_{VV}) S_{HV}^* \rangle)}{\langle |S_{HH} - S_{VV}|^2 \rangle + 4\langle |S_{HV}|^2 \rangle} \right) + \pi \right] \quad 4.24$$

where, Re is real part, ρ is Angle shift in the orientation and the estimated orientation angle (OA) ranges from $-\frac{\pi}{4}$ to $\frac{\pi}{4}$

In the formula of coherency matrix elements

$$\theta = \frac{1}{4} \left[\tan^{-1} \left(\frac{2\text{Re}(T_{23})}{T_{22} - T_{33}} \right) + \pi \right] \quad 4.25$$

$$[t] = [U][T][U^T] \quad 4.26$$

$$[U] = \begin{bmatrix} 1 & 0 & 0 \\ 0 & \cos 2\theta & \sin 2\theta \\ 0 & -\sin 2\theta & \cos 2\theta \end{bmatrix} \quad 4.27$$

$[t]$ is Coherency matrix after POA shift and U is Rotation matrix

5. MODELING APPROACH: WATER CLOUD MODEL (WCM) AND EXTENDED WATER CLOUD MODEL (EWCM)

5.1. WATER CLOUD MODEL

WCM, developed by (Attema and Ulaby, 1978), can be simply described as the backscatter of the forest as the sum of backscatter from vegetation and ground. The model expects the vegetation acting like a cloud filled with water droplets over a flat ground surface. The backscatter received is modelled as water droplets (Attema and Ulaby, 1978) (Kumar et al., 2012). The incident wave interact with target and incompletely return to the sensor, incompletely pass on to lower vegetation layer due to attenuation (when EM waves interact with canopy and canopy gaps, and that time some EM wave are loss i.e. called attenuation) and rest reflected back from ground. This can be mathematically described as (Kumar et al., 2012).

$$\sigma_{for}^0 = \sigma_{veg}^0 + \sigma_{gr}^0 T_{tree} \quad 5.1$$

where σ_{for}^0 is forest backscatter, σ_{veg}^0 is backscatter of vegetation, σ_{gr}^0 is backscatter of ground and T_{tree} is two way tree transmissivity.



Figure 5-1: Backscatter of ground σ_{gr}^0 and backscatter of vegetation σ_{veg}^0

Transmissivity is the quantifiable assessment of the capacity of electromagnetic waves to move inside and outside of the canopy gaps. The transmissivity depends on the amount of ground backscatter getting through the canopy. Backscattering of ground will be reduced in a dense forest as compared to an open forest and therefore the transmissivity of dense forest will be considered low. In the transmissivity assessment wavelength is the important feature. If wavelength is longer, the transmissivity will be higher. Praks et al., (Praks et al., 2007) defined the equation

$$T = \frac{\beta_{gc}}{\beta_{go}}$$

where β_{gc} backscattering from ground with canopy gaps and β_{go} is backscattering from ground without canopy gaps.

The model expects the vegetation layer as homogeneous medium. Double bounce, associated with interaction of microwave with ground or stem is not considered, so is the scattering through canopy gaps (Kumar, 2009) (Santoro et al., 2003) (Santoro et al., 2006). The model was further developed by Askene et al., (Askne et al., 1995) by including the gaps in the canopy by introducing the area fill factor (μ).

$$\mu = \frac{1 - e^{-\beta B}}{1 - e^{-\sigma h}} \quad 5.2$$

where, B is above ground biomass, $e^{-\beta B} = T_{for}$ and $e^{-\sigma h} = T_{tree}$ demonstrating transmissivity of forest and tree correspondingly.

Hence the model can now be represented as

$$\sigma_{for}^0 = (1 - \mu)\sigma_{gr}^0 + \mu[\sigma_{gr}^0 T_{tree} + \sigma_{veg}^0(1 - T_{tree})] \quad 5.3$$

Here $(1 - \mu)\sigma_{gr}^0$ is demonstrating backscatter from ground through canopy gaps with $(1 - \mu)$ demonstrating open ground. $\mu \sigma_{gr}^0 T_{tree}$ demonstrating backscatter from ground through canopy and $\mu \sigma_{veg}^0(1 - T_{tree})$ demonstrating backscatter through vegetation (Kumar et al., 2012).

The two way tree transmissivity T_{tree} can be written in positions of attenuation per meter α and thickness of attenuating layer h as

$$\sigma_{for}^0 = (1 - \mu)\sigma_{gr}^0 + \mu[\sigma_{gr}^0 e^{-\alpha h} + \sigma_{veg}^0(1 - e^{-\alpha h})] \quad 5.4$$

Rearranging the equation

$$\sigma_{for}^0 = [(1 - \mu) + \mu e^{-\alpha h}]\sigma_{gr}^0 + \mu\sigma_{veg}^0(1 - e^{-\alpha h}) \quad 5.5$$

As SAR image cannot be used to retrieve the transmissivity of a particular tree, transmissivity of a patch is deliberated, represented as T_{for} . T_{for} can be represented in terms of area fill factor as (Santoro et al., 2003).

$$T_{for} = [(1 - \mu) + \mu e^{-\alpha h}] \quad 5.6$$

If α is very large, above equation becomes

$$T_{for} = [(1 - \mu) + \mu e^{-\alpha h}] \approx (1 - \mu) \quad 5.7$$

Hence,

$$\sigma_{for}^0 = T_{for}\sigma_{gr}^0 + \sigma_{veg}^0(1 - T_{for}) \quad 5.8$$

Hence, equation 5.1 becomes equation 5.9 due to strong attenuation resulting in large(σ)(Santoro et al., 2003).

$$\mu = 1 - e^{-\beta B} \quad 5.9$$

Also, T_{for} now can be written as

$$T_{for} = e^{-\beta B} \quad 5.10$$

This quantifies the total backscatter from forest as (Kumar, 2009) (Santoro et al., 2006) (Santoro et al., 2003).

$$\sigma_{for}^0 = \sigma_{gr}^0 e^{-\beta B} + \sigma_{veg}^0 (1 - e^{-\beta B}) \quad 5.11$$

By utilize equation 5.6 and 5.10 it can be derive that:

$$e^{-\beta B} = (1 - \mu) + \mu e^{-\alpha h} \quad 5.12$$

Now empirically defined coefficient (β) can be derived as

$$\beta = -\frac{1}{B} \ln \left[\frac{\sigma_{for}^0 - \sigma_{veg}^0}{\sigma_{gr}^0 - \sigma_{veg}^0} \right] \quad 5.13$$

5.2. EXTENDED WATER CLOUD MODEL

Double bounce scattering due to ground stem should be considered for accurate biomass estimation which is not modelled in WCM. EWCM takes these interactions into consideration. The double bounce from ground stem interaction passing through canopy gaps is deliberated as (Poolla, 2013)

$$(1 - \mu)\sigma_{gs}^0 \quad 5.14$$

Here, $(1 - \mu)$ represents canopy free ground and σ_{gs}^0 is ground stem backscatter.

The double bounce from ground stem interaction passing through canopy is considered as

$$\mu\sigma_{gs}^0 T_{tree} \quad 5.15$$

So, EWCM for higher order interaction becomes

$$\sigma_{for}^0 = (1 - \mu)\sigma_{gr}^0 + \mu\sigma_{gr}^0 T_{tree} + \mu\sigma_{veg}^0 (1 - T_{tree}) + (1 - \mu)\sigma_{gs}^0 + \mu\sigma_{gs}^0 T_{tree} \quad 5.16$$



Figure 5-2: Ground stem backscatter (σ_{gs}^0) from the canopy gaps



Figure 5-3: Ground stem backscatter (σ_{gs}^0) through the canopy gaps

Replacing two way tree transmissivity in terms of attenuation per meter and thickness of attenuating layer, the above equation becomes (Poolla, 2013).

$$\sigma_{for}^0 = (1 - \mu)\sigma_{gr}^0 + \mu\sigma_{gr}^0 e^{-ah} + \mu\sigma_{veg}^0(1 - e^{-ah}) + (1 - \mu)\sigma_{gs}^0 + \mu\sigma_{gs}^0 e^{-ah} \quad 5.17$$

$$\sigma_{for}^0 = \sigma_{gr}^0[(1 - \mu) + \mu e^{-ah}] + \mu\sigma_{veg}^0(1 - e^{-ah}) + \sigma_{gs}^0[(1 - \mu) + \mu e^{-ah}] \quad 5.18$$

$$T_{for} = [1 - \mu + \mu e^{-ah}] \quad 5.19$$

EWCM equation is accessible as

$$\sigma_{for}^0 = \sigma_{ar}^0 T_{for} + \sigma_{veg}^0(1 - T_{for}) + \sigma_{as}^0 T_{for} \quad 5.20$$

T_{for} , can be written in the form of empirically defined coefficient (β) and above ground biomass (B) (Poolla, 2013).

$$\sigma_{for}^0 = \sigma_{ar}^0 e^{-\beta B} + \sigma_{veg}^0(1 - e^{-\beta B}) + \sigma_{as}^0 e^{-\beta B} \quad 5.21$$

Four unknown parameter (σ_{for}^0 , σ_{gr}^0 , σ_{veg}^0 and σ_{gs}^0) are there in this above equation 5.21. Polarimetric decomposition were utilized to find these unknown parameters. Three parameters (surface scattering, double bounce and volume scattering) are retrieved from scattering information. The fourth parameter (β), was calculated with the help of 15 plots of which the field biomass was already known using EWCM approach. After that find the all the unknown parameter to estimate the AGB.

6. RESULT AND DISCUSSION

This chapter concerns with the results achieved using the adopted methodology. The present research work was attempted to estimate above ground biomass using semi-empirical modelling approach (EWCM). The outcomes corresponds to the objectives enlisted in chapter one. PolInSAR based coherency matrix was used in this study. PolInSAR image was generated through the co-registration of the master and slave images. Deorientation process was applied to PolInSAR imagery and the effect of this de-orientation process was examined on the obtained results. Polarimetric decomposition modelling was used to obtain the scattering elements i.e. volume scattering, double-bounce scattering and surface scattering. This information was used to derive parameters required for semi-empirical modelling i.e. EWCM for the AGB estimation. Field data was also collected for the validation. The model derived biomass was compared with the field biomass. Accuracy assessment was accomplished using two statistical parameters i.e. coefficient of determination (R^2) and root mean square error (RMSE) to judge the potential of modelling approach.

6.1. RELATION BETWEEN FIELD ESTIMATED AGB AND VOLUME SCATTERING RETRIEVED FROM SAR IMAGES

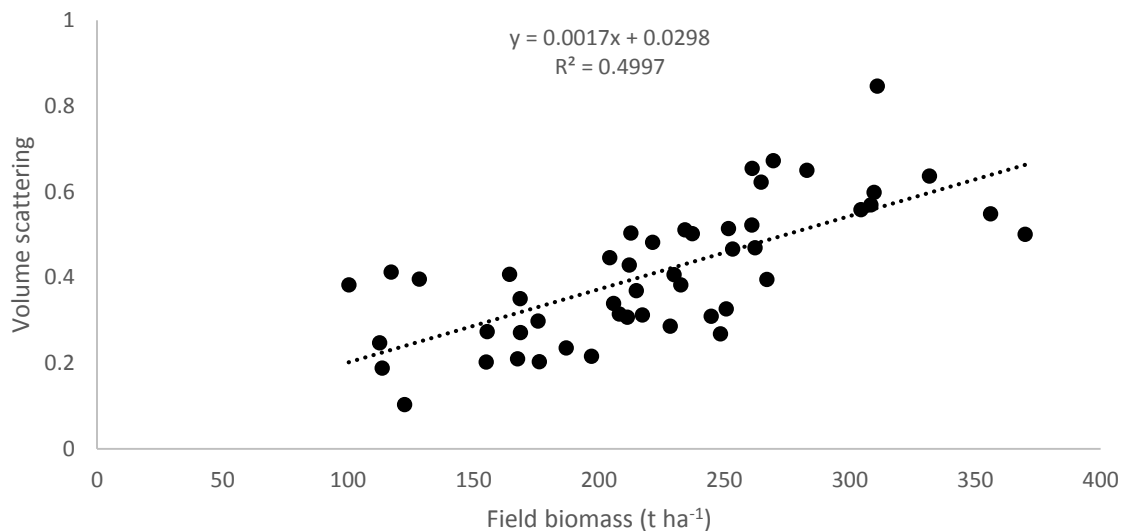


Figure 6-1: Linear regression between field biomass (x axis) and volume scattering (y axis) of master image for 49 locations of field plots (28th January 2014)

Regression analysis was performed to find out the relationship between volume scattering and the field measured biomass for the master image. It is clearly seen in the figure 6-1 that increase in volume scattering corresponds to increase in field biomass. This shows the positive correlation between the two variables i.e. volume scattering and the field biomass. In the above figure, some forest plots report high biomass but the corresponding volume scattering show low values and some plots report low biomass but volume scattering show high values. The cause of this tendency is due to the sensor orientation and forest canopy thickness.

Coefficient of determination (R^2) between field biomass against volume scattering comes out to be 0.499 for the master image. Volume scattering values for most of the points lies in the range 0.2 to 0.6.

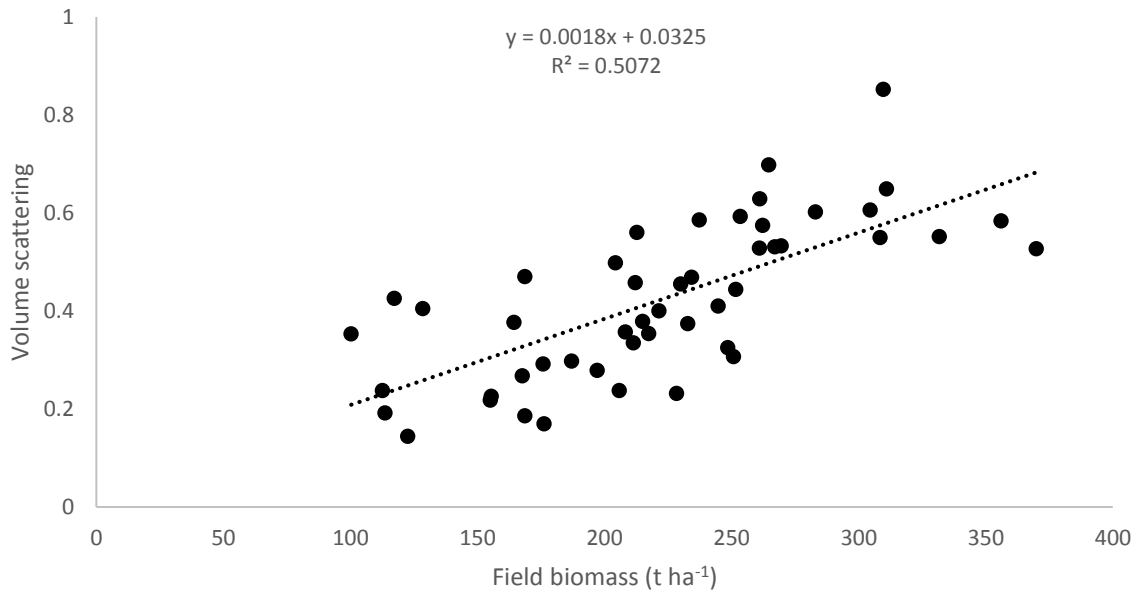


Figure 6-2: Linear Regression between field biomass (x axis) and Volume scattering (y axis) of slave image for 49 locations of field plots (20th February 2014)

Regression analysis was done for the slave image as well. Figure 6-2 shows correlation between field biomass (x axis) and volume scattering (y axis) for slave imagery calculated for 49 locations of field plots (20th February 2014). The scatter plot shows that value of volume scattering escalates when the field biomass increases. But some of the plots reports higher volume scattering even when biomass is low and some plots show low volume scattering in spite of high biomass value. Slave volume scattering depicts higher value of coefficient of determination (R^2) i.e. 0.5072 as compared to the master volume scattering. Both the plots show approximately equal correlation and most of the volume scattering values lies in the range 0.2 to 0.6. Various studies (Chandola, 2014) have calculated the biomass of the vegetation using volume scattering separately for slave and master images but this study approaches the subject by first combining the master and slave images using PolInSAR based coherency matrix and then calculating the biomass using semi-empirical model i.e. EWCM. Table 6-1 depicts values of coefficient of determination between volume scattering against field biomass for master and slave images.

Table 6-1: Estimated R^2 value between volume scattering and field biomass of SAR images

Coefficient of determination	Master image	Slave image
(R^2)	0.4997	0.5072

6.2. SAR IMAGES (GRAY IMAGES)

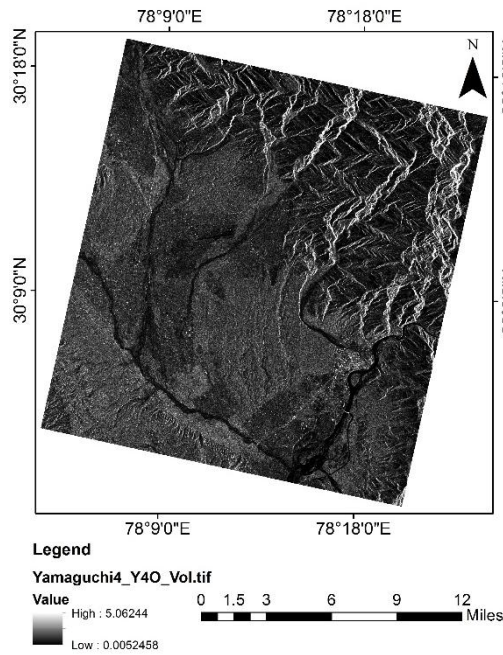


Figure 6-3: Volume scattering for master image

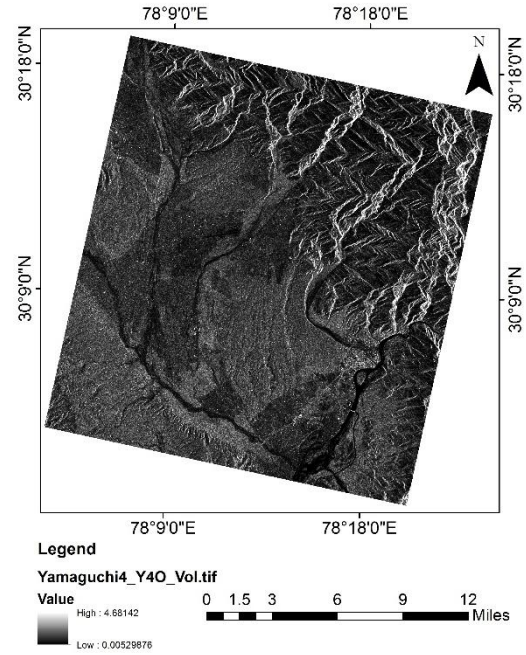


Figure 6-4: Volume scattering for slave image

Figure 6-3 shows the volume scattering for master image and figure 6-4 shows the volume scattering for slave image. Both the images were acquired on different dates and do not show similar value of coefficient of determination. The volume scattering for slave image shows the R^2 value as 0.50 and the volume scattering for master image shows R^2 value as 0.4997.

6.3. SURFACE AND DOUBLE BOUNCE SCATTERING FOR POLINSAR IMAGE

The first element of coherency matrix i.e. T11 component as shown in equation 4.6 did not significantly change after applying the deorientation. It is observed that the element is roll-invariant and T11 component of the matrix doesn't change. The T11 component signifies the surface scattering component. Hence deorientation process does not significantly improve the previously computed values. To study the result of deorientation on the surface scattering element, 49 plots from the field measurement were taken which are shown in the figure 6-5.

Figure 6-5 shows the value of the surface scattering of PolInSAR image before and after de-orientation. Black line and green line shows the surface scattering values after and before deorientation respectively. The graphs indicates that the surface scattering increases after de-orientation despite the fact that the T11 component is invariant. The modelling of surface scattering which incorporates different components

alongside the T11 is the reason behind the decrement in this quantity (as above mentioned in fourth chapter).

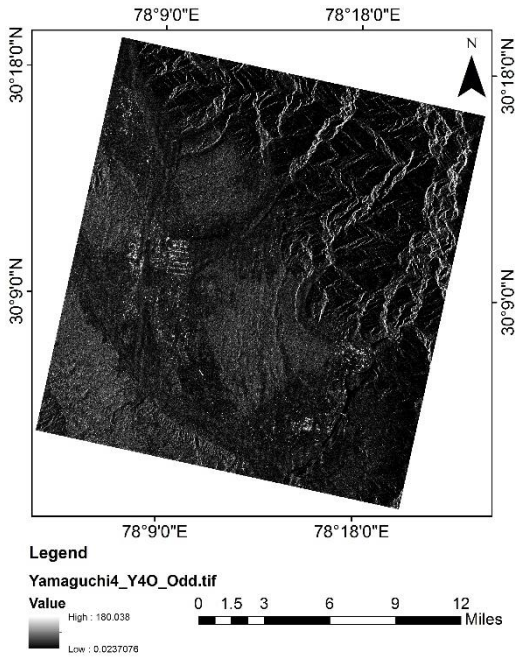


Figure 6-5: Surface scattering of PolInSAR image

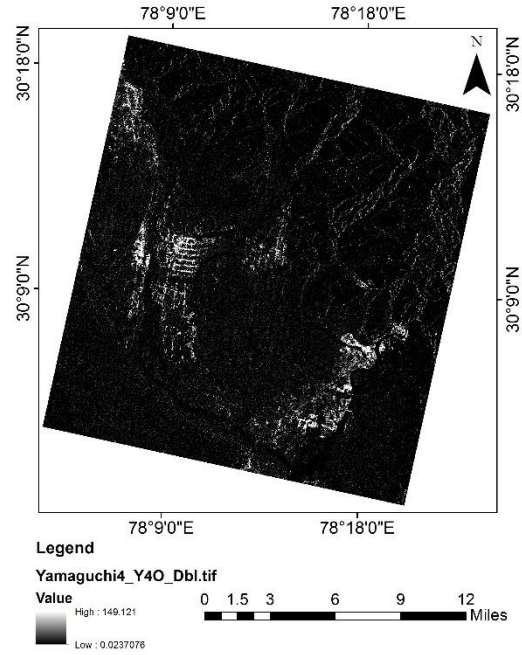


Figure 6-6: Double bounce of PolInSAR image

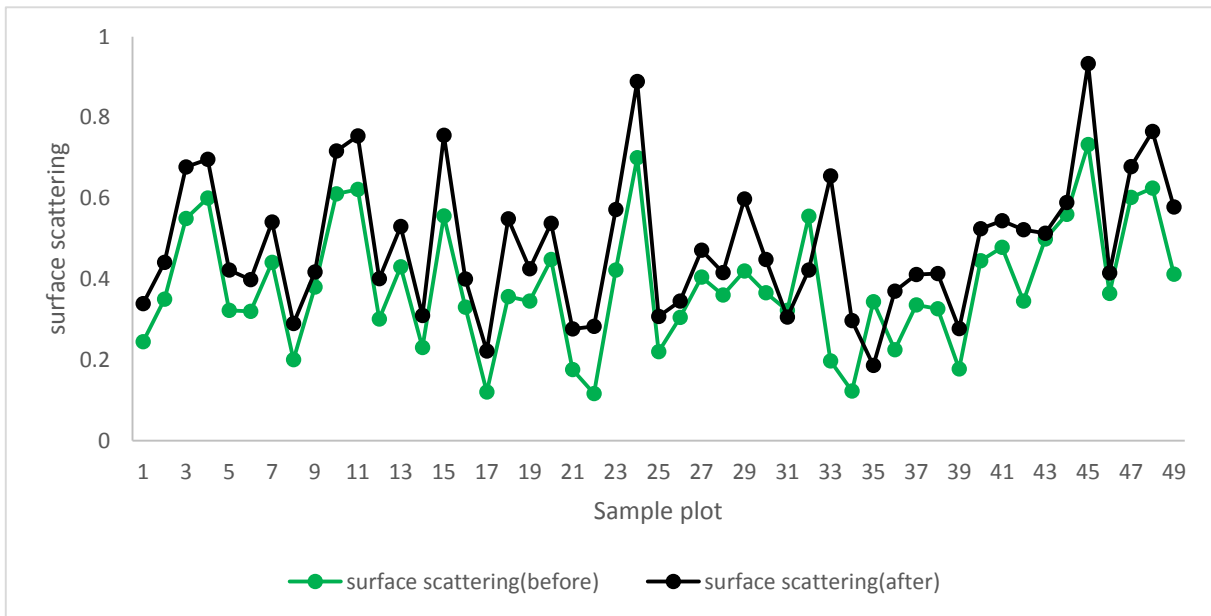


Figure 6-7: Surface scattering before and after-deorientation

T22 component of the coherency matrix as shown in equation 4.6 did not significantly change after applying the deorientation. It is observed that T22 component is roll-invariant and hence does not change. The T22 component represents the double bounce scattering mechanism. Hence deorientation does not significantly alter its values. To study the result of deorientation on the double-bounce element, 49 plots from the field measurement were utilized.

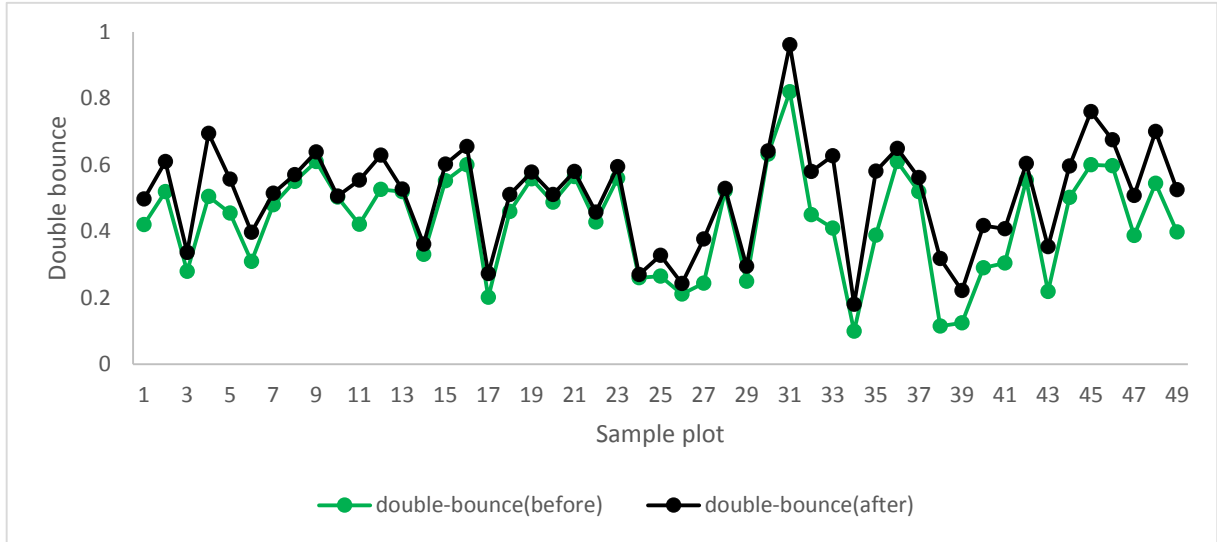


Figure 6-8: Double-bounce scattering before and after deorientation

The backscatter from double bounce scattering for before and after deorientation is as shown in figure 6-8. Here the black and green lines shows the values of after and before deorientation respectively. There is an increment in double-bounce scattering after de-orientation.

6.4. POLINSAR VOLUME SCATTERING (BEFORE AND AFTER DE-ORIENTATION)

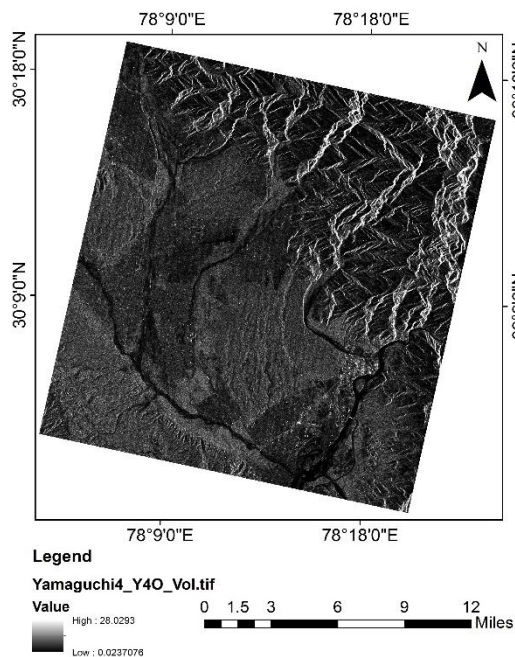


Figure 6-9: PolInSAR based Volume scattering (before de-orientation)

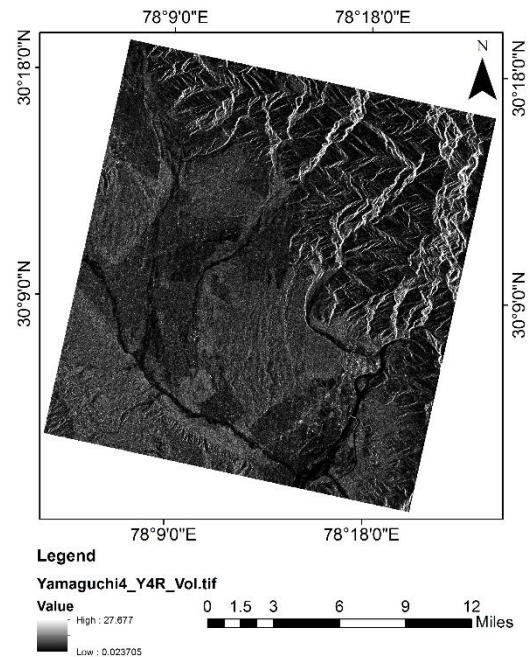


Figure 6-10: PolInSAR based Volume scattering (after de-orientation)

Figure 6-9 and figure 6-10 shows PolInSAR volume scattering elements for both before and after deorientation. De-oriented PolInSAR image shows less volume scattering values than the values of image

before de-orientation (as shown in figure 6-13). Forty nine plots were taken from the field data to analyse the effect of deorientation. The polarization orientation angle shift was compensated using equation 4.23 to minimize the overestimation of volume scattering. After applying the deorientation process, the overall influence of volume scattering was reduced to a certain extent in every plot.

6.5. RELATION BETWEEN FIELD ESTIMATED AGB AND VOLUME SCATTERING OF POLINSAR DATA

POLINSAR VOLUME SCATTERING (BEFORE DE-ORIENTATION)

First of all the SAR images were combined using PolInSAR based coherency matrix. The PolInSAR image was subjected to deorientation. Regression analysis was carried out for the PolInSAR image before deorientation. Before de-orientation of PolInSAR, figure 6-11 depicts that the volume scattering varies linearly with field biomass. Field biomass and volume scattering shows value of coefficient of determination (R^2) as 0.589. The deorientation equation is used for PolInSAR based coherency matrix. Coherency matrix is utilized in Yamaguchi decomposition after deorientation process. Four decomposition mechanism generated surface, double-bounce, volume and helix scattering but the results attained are mainly contributed by a decomposition component i.e. volume scattering from the forest canopy cover. After de-orientation of PolInSAR based coherency matrix, $T_{33} = 4|S_{HV}|^2$ element gets reduced which is a cross-polarized element. Due to the decrease in T_{33} element, volume scattering also decreases.

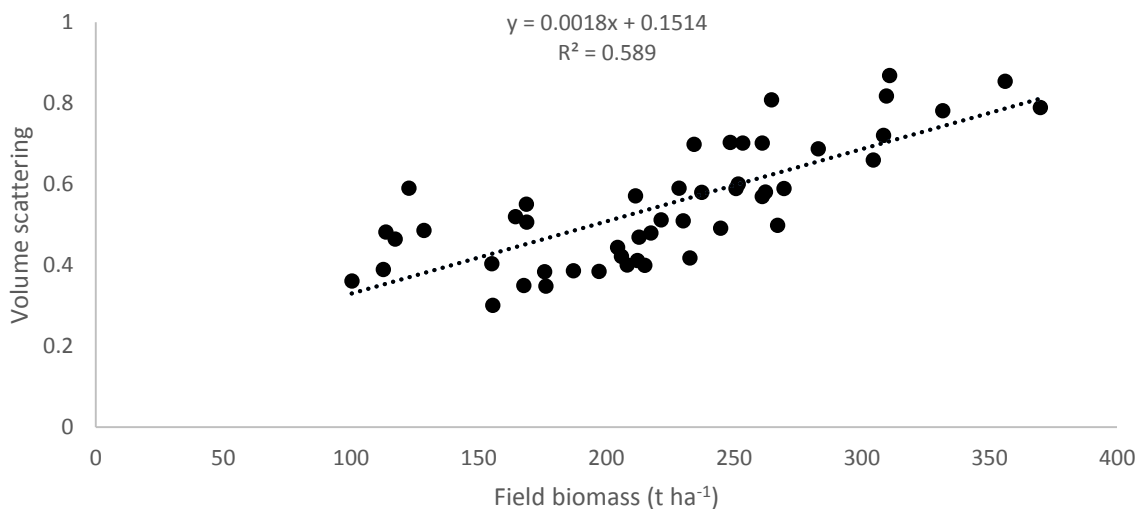


Figure 6-11: Linear regression between field biomass (x axis) and Volume scattering (y axis) of PolInSAR image for 49 locations of field plots (before de-orientation)

POLINSAR VOLUME SCATTERING (AFTER DE-ORIENTATION)

After deorientation PolInSAR volume scattering shows low correlation as compared to before deorientation PolInSAR volume scattering. This study utilized after-deorientation PolInSAR volume scattering image.

This is because the results does not rely upon higher correlation values for precise biomass estimation but on the certainty of elements participating in the scattering. This information retrieval is easier from after-deorientation procedure carried out on PolInSAR image.

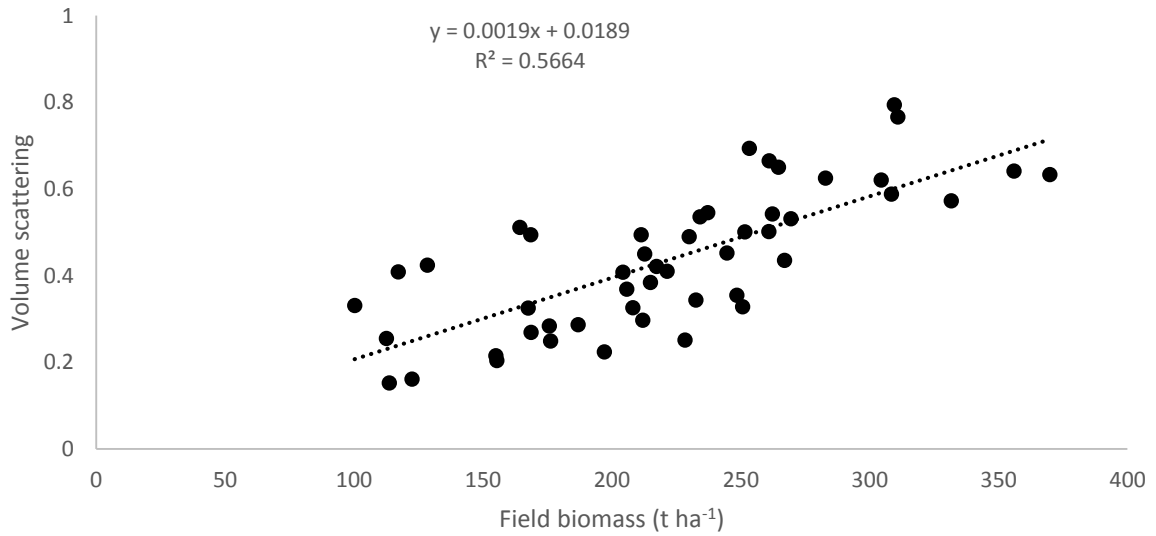


Figure 6-12: Linear regression between field biomass (x axis) and Volume scattering (y axis) of PolInSAR image for 49 locations of field plots (after de-orientation)

This study utilizes after-deorientation PolInSAR image to acquire all the scattering information which acts as the input for EWCM. Both figure (6-11) and (6-12) shows that for the volume scattering values ranging from 0.2 to 0.8 field biomass values lies in the range 150 (t ha⁻¹) to 270 (t ha⁻¹). The combination of two images i.e. PolInSAR image shows higher correlation value as compared to SAR images (master and slave images).

Table 6-2: Estimated R² value between volume scattering and field biomass for the PolInSAR image before and after de-orientation

R ² values of PolInSAR image	
Before de-orientation	After de-orientation
0.589	0.5664

6.6. COMPARISON VALUE OF POLINSAR IMAGE BEFORE AND AFTER DE-ORIENTATION

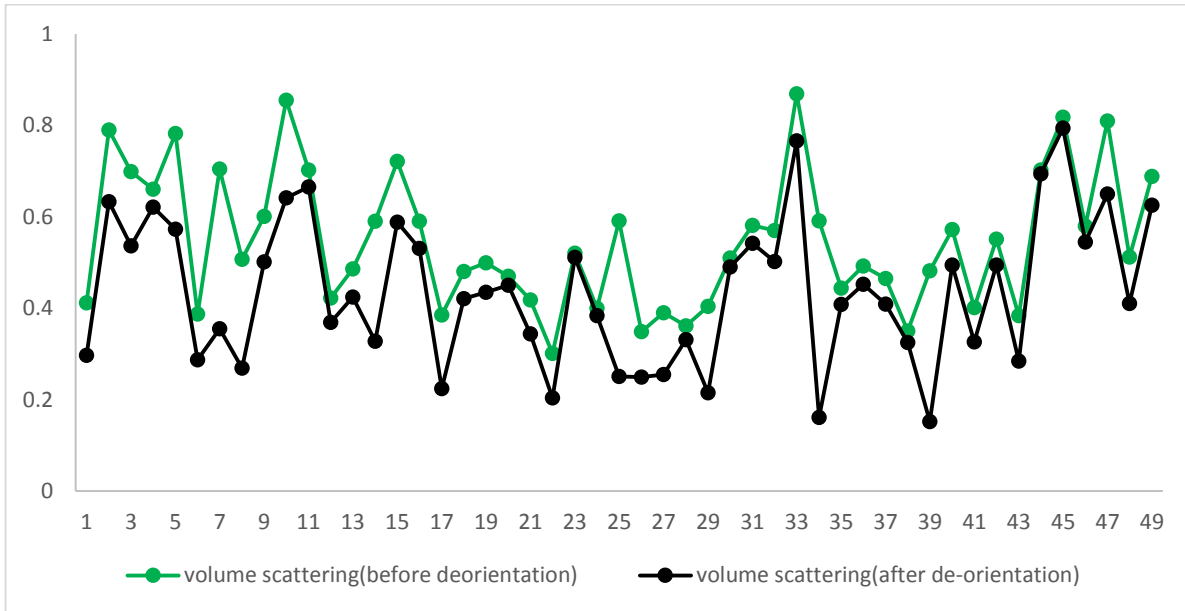


Figure 6-13: Volume scattering values before and after de-orientation of PolInSAR image

Figure 6-13 shows the contrast in volume scattering (y axis) value in 49 sample plot (x axis), before and after deorientation for PolInSAR image. The green line shows that value of volume scattering before deorientation and the black line shows that the value of volume scattering after deorientation.

6.7. RGB IMAGE OF POLINSAR IMAGE (BEFORE AND AFTER DE-ORIENTATION)

Figure 6-14 and 6-15 shows before and after deorientation PolInSAR RGB images. De-oriented image provides low scattering value and high double bounce scattering due to overestimation of volume scattering and underestimation of double bounce scattering than before-deorientation images. This can be easily visually interpreted from the amount of either red (representing double bounce scattering) or green (representing volume scattering) colour in the circular highlighted area of the image.

The rectangular highlighted area shows a more pronounced effect for the same deorientation effect applied over the image showing urban area contributing more double bounce rather than volume scattering. This is primarily due to non-alignment of the satellite to the urban structures. However after deorientation the amount double-bounce has clearly increased for the urban area hence confirming the effect of over estimation of volume scattering without deorientation.

Figure 6-16 shows the graph for volume scattering (y-axis) value for master, slave and PolInSAR image. The red line shows the value of master image volume scattering, black line shows the value of slave image volume scattering and blue line shows the value of PolInSAR image volume scattering. The PolInSAR image has been selected in EWCM modelling because it provides more accurate scattering information than either of

master or slave image. Coefficient of determination (R^2) value is higher for PolInSAR image than for master and slave image for same AGB calculated from field plots.

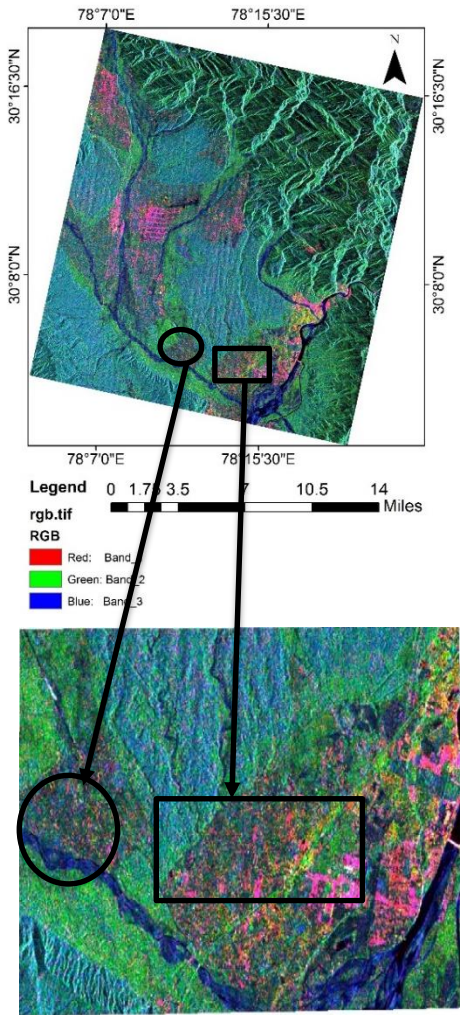


Figure 6-14: PolInSAR RGB image before deorientation

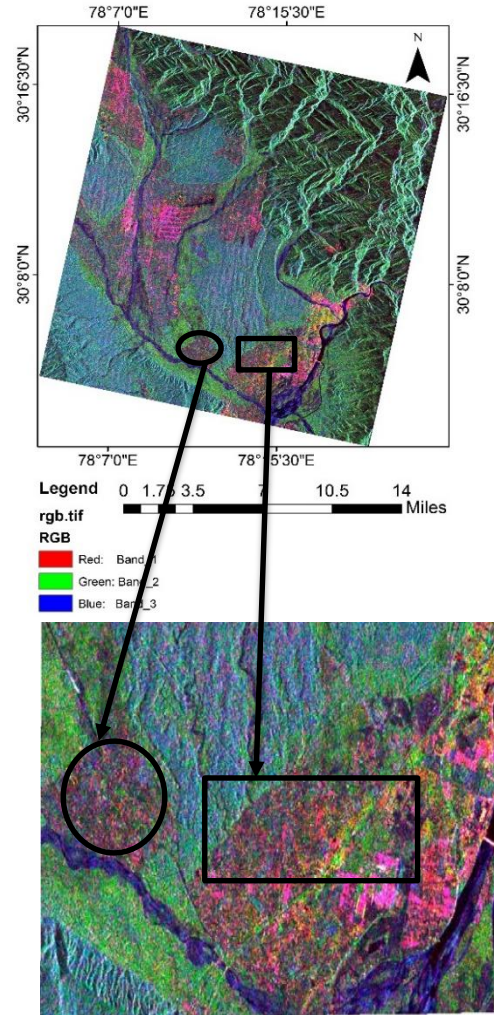


Figure 6-15: PolInSAR RGB image after deorientation

Master, slave and PolInSAR volume scattering

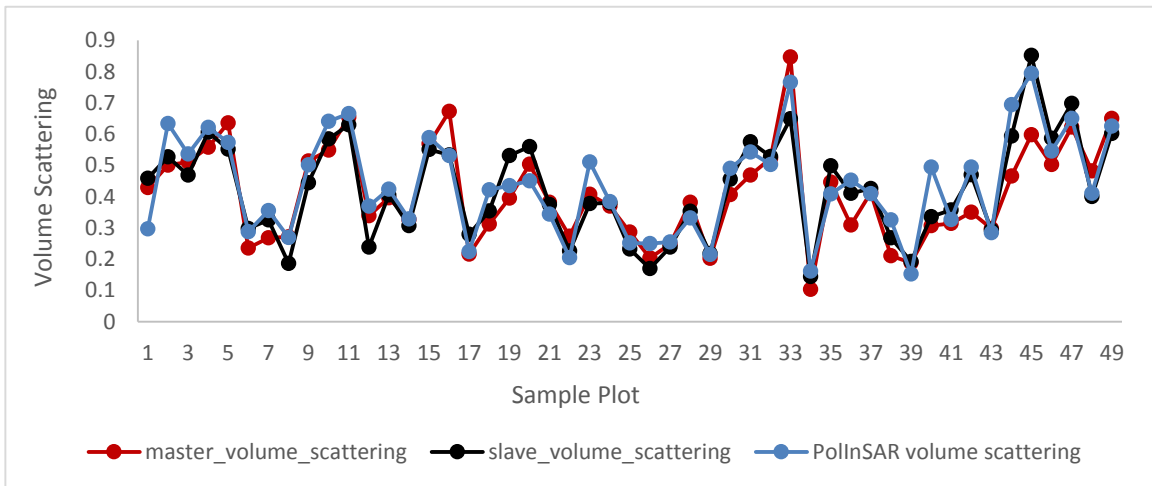


Figure 6-16: Volume scattering for master, slave and PolInSAR image for 49 locations of field plots

6.8. BIOMASS ESTIMATION FROM EWCM

The semi-empirical model i.e. EWCM is defined in chapter 5. Modelled AGB equation (6.4) was used to estimate biomass. The results are shown in following sections.

Field AGB and Modelled AGB

Figure 6-17 shows the linear regression between field AGB and modelled biomass. The R^2 value is 0.47, the modelled AGB show RMSE equal to 55.18 ($t\ ha^{-1}$) and accuracy for model output is 72.13%. Equation 5.21 is utilized for the estimation of modelled biomass. RMSE is calculated utilizing the formula as given in equation (6.1).

$$RMSE = \sqrt{\frac{\sum_{i=1}^N (\text{measured biomass} - \text{estimated biomass})^2}{N}} \quad 6.1$$

where, measured biomass is modelled biomass, estimated biomass is field biomass and N is the number of sample plots utilized in modelled biomass. Percent accuracy is calculated utilizing the formula in equation 6.2.

$$\text{Percent Accuracy} = \left[1 - \frac{1}{N} \sum_{i=1}^N \frac{(\text{measured biomass} - \text{estimated biomass})}{\text{estimated biomass}} \right] \times 100 \quad 6.2$$

The precision of the modelled estimated biomass explains the relevance of the modelling procedure as it demonstrates how close the model estimated biomass to the field estimated biomass. The Percent accuracy was achieved as 72.13% for the measured biomass.

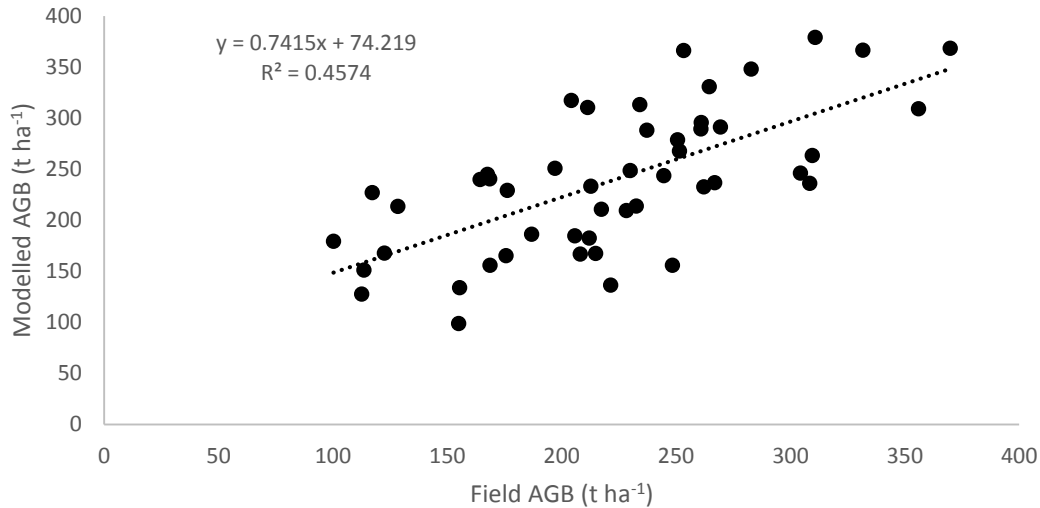


Figure 6-17: Co-relation between field AGB (x axis) and modelled AGB (y axis) for 49 plots

Retrieval of β value for estimation of modelled biomass

Some plots (15 plots) of the field data were used for estimation of semi-empirically defined coefficient β and remaining 34 plots were used for accuracy assessment. Equation 6.3 was utilized to find β value for

the estimation of modelled biomass. This equation shows the empirically defined coefficient (β) and above ground biomass (B)

$$\beta = -\frac{1}{B} \ln \left(\frac{\sigma_{for}^0 - \sigma_{veg}^0}{\sigma_{gr}^0 - \sigma_{veg}^0 + \sigma_{gs}^0} \right) \quad 6.3$$

$$B = -\frac{1}{\beta} \ln \left(\frac{\sigma_{for}^0 - \sigma_{veg}^0}{\sigma_{gr}^0 - \sigma_{veg}^0 + \sigma_{gs}^0} \right) \quad 6.4$$

where, σ_{for}^0 is forest backscatter, σ_{veg}^0 is backscatter of vegetation, σ_{gr}^0 is backscatter of ground and σ_{gs}^0 backscatter of interact of ground and stem. Empirically defined coefficient (β) is calculated by utilizing the field data information. R^2 comes out to be 0.5299 for β (as shown in fig 6-18).

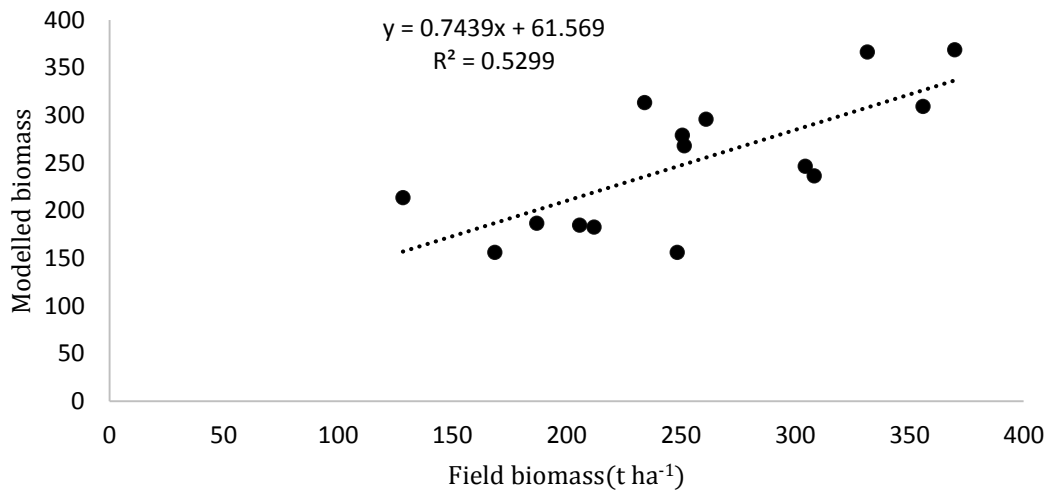


Figure 6-18: Linear regression between field biomass against modelled biomass for the 15 plots

Figure 6-18 shows the linear regression between field biomass and modelled biomass for the 15 plots were used for calculation of empirically defined coefficient value. From the 15 plots, correlation coefficient value was observed to be 0.0024. The R^2 between modelled biomass and the field biomass was 0.5299 for the fifteen plots. The field biomass was utilized for the validation of modelled biomass. The table 6-3 indicates RMSE value equal to 50.17 (t ha⁻¹) and percent accuracy of 78.6 for 15 plots. These 15 plots show higher accuracy as compared to the remaining 34 plots.

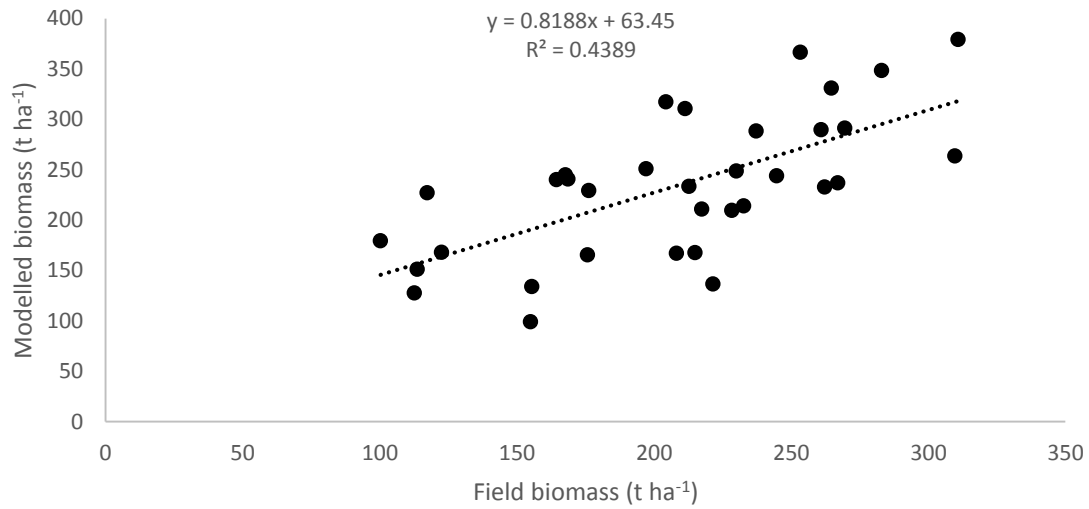
Modelled biomass for the remaining 34 plots

Figure 6-19: Linear regression between modelled biomass (y axis) and field biomass (x axis) for the thirty four plots.

Figure 6-19 shows the linear regression between field biomass and modelled biomass for the 34 plots to estimate the above ground biomass. The coefficient of determination R^2 between the modelled biomass against the field biomass came out to be 0.438. This graph also shows that most of the value of modelled biomass varies from 150 ($t\ ha^{-1}$) to 300 ($t\ ha^{-1}$). The remaining 34 plots gives RMSE of 58.8 ($t\ ha^{-1}$) and percent accuracy of 69.09%.

Table 6-3: R^2 , RMSE and Percent Accuracy obtained for modelled AGB

Modelled AGB								
Total forty nine plots			Fifteen plots			Thirty four plots		
R^2 value	RMSE ($t\ ha^{-1}$)	Percent Accuracy	R^2 value	RMSE ($t\ ha^{-1}$)	Percent Accuracy	R^2 value	RMSE ($t\ ha^{-1}$)	Percent Accuracy
0.47	55.18	72.13	0.52	50.17	78.6	0.43	58.8	69.09

Table 6-3 shows the R^2 , RMSE and percent accuracy for the modelled AGB. The estimated AGB using EWCM is showing reasonable accuracy when the de-oriented PolInSAR image are used. The EWCM Modelled AGB has an RMSE of 55.18 ($t\ ha^{-1}$) and a percent accuracy of 72.13%. Semi empirically defined coefficient β is used for the fifteen plot and shows RMSE of 50.17 ($t\ ha^{-1}$) and a percent accuracy of 78.6%. Remaining 34 plots are utilized for estimated AGB and shows RMSE of 58.8 ($t\ ha^{-1}$) and percent accuracy of 69.09%.

7. DISCUSSION

The key objective of this research work was to explore the potential of PolInSAR based scattering retrieval for semi-empirical modelling (EWCM) of forest above ground biomass. The main aim of this section is to provide interpretations of the results obtained following the given methodology. The discussion is divided into four parts based on each of the objectives.

The first objective deals with the generation of PolInSAR based 3×3 coherency matrix elements for decomposition. The coherency matrix was modified for the PolInSAR image with master and slave image according to the coherency matrix of the PolSAR image (Yamaguchi et al., 2011). Here we are dealing with the PolInSAR image coherency matrix with Pauli vector of master and slave. Hence, to make this matrix hermitian we needed to make some assumptions about the data. The results are not affected as we are trying to make the coherency matrix as hermitian which on applying decomposition will give scattering elements. SAR images (master and slave images) were decomposed using Yamaguchi four component decomposition technique. PolInSAR based coherency matrix generated by co-registration of SAR images (master and slave images). Figure 6-11 and figure 6-12 shows the relation between field AGB and PolInSAR based volume scattering. It is clearly seen from the figures (figure 6-11 and figure 6-12) that very less difference (0.02 approximately) in coefficient of determination was obtained after de-orientation of PolInSAR coherency matrix. Previous research by Chandola (Chandola, 2014) was done for biomass estimation in which coefficient of determination for master image before and after de-orientation was found to be 0.457 and 0.433 respectively. For slave image R^2 before and after de-orientation was 0.471 and 0.474 respectively. In the current study, SAR images reported R^2 value of 0.4905 and 0.5062 respectively but de-oriented PolInSAR image show R^2 value of 0.5575. Hence, it can be said that a reliable scattering was obtained using a de-oriented PolInSAR image. The PolInSAR image after de-orientation provides high double bounce scattering values and low volume scattering due to overestimation of volume scattering and underestimation of double bounce scattering.

The second objective deals with the retrieval of scattering information through PolInSAR based decomposition modelling. The scattering information retrieved from the PolInSAR based decomposition modelling is shown in figure (6-5), (6-6), (6-9) and (6-10). The values of surface scattering and double bounce scattering were quite high after deorientation process as it was affected by tree orientation and canopy thickness. Whereas after deorientation, the values for volume scattering decreases as de-orientation process removes overestimation of volume scattering.

The third objective concerns the estimation of AGB using a semi-empirical modelling approach i.e. EWCM. Three parameters i.e. surface scattering, double bounce and volume scattering were retrieved from the

scattering information. The field biomass for 15 plots along with the EWCM approach was used to obtain fourth parameter (β). AGB was estimated with help of model inversion of EWCM as shown in equation 5.21.

The fourth objective compares the model estimated biomass with the actual field biomass. The regression analysis was done for the modelled biomass against the field biomass. For the accuracy assessment statistical parameter such as RMSE as well as percentage accuracy was used. The scatter plot was generated for 49 plots between the biomass estimated from EWCM and the field biomass. The same procedure was followed for the 15 plots and 34 plots as well. All the three scatter plots shows a positive correlation between the biomass estimated from EWCM and the field biomass. The highest coefficient of determination (R^2) was found to be 0.5299 for the 15 plots.

The EWCM (as mentioned in the chapter 5) utilized de-oriented PolInSAR image to retrieve scattering mechanism of forest AGB. EWCM included one extra parameter than WCM (as mentioned in the chapter 5) i.e. ground stem interaction. The parameters derived by utilising EWCM using various decomposition components and AGB have already been explained in the chapter 6. In this study reliable scattering information was achieved utilizing de-oriented PolInSAR image (as shown in fig 6-12). 72% percent accuracy and 55.18 ($t\ ha^{-1}$) RMSE was found for AGB using field data.

In this research work fully polarimetric data was utilized. Fully polarimetric data contains all type of scattering information that is needed in the EWCM model. The main purpose of using fully polarimetric SAR data is lesser ambiguity for scatterer information and site dependence which is better than in situ measurement for every scatterer which is very time consuming. However the uncertainties in the stem-volume volumetric equation (Forest Survey of India, 1996) and specific gravity data are the factors which can be further improved upon. As destructive sampling is prohibited in India and there is also limited amount of time for research, the data provided by FSI is the only feasible option available. The accuracy from GPS readings is very low which is compensated by taking the reading over homogeneous plots.

The impact of POA shift on the PolInSAR data pair was also tested and effect of POA compensation on polarimetric decomposition modelling was analysed. The shift in POA may occur due to the shape and orientation of the object. Overestimation in volume scattering and underestimation of double-bounce scattering was recorded as a result due to shift of POA. Deorientation was performed by rotating the coherency matrix elements (T_{11} , T_{22} , and T_{33}). Decrease in volume scattering and increase in double bounce scattering was obtained from the decomposed based PolInSAR based coherency matrix. Equation (4.25) is used for the estimation of orientation angle shift. POA shift compensated image was implemented on the PolInSAR pair. R^2 value between volume scattering and field biomass for PolInSAR image before de-orientation and after de-orientation is 0.5897 and 0.5664 respectively. Deorientation leads to better

estimation of the amount of volume scattering actually taking place, which is the main component for biomass estimation.

The estimated AGB using EWCM shows reasonable accuracy when the de-oriented PolInSAR image was used. The EWCM Modelled AGB had an RMSE of 55.18 (t ha⁻¹) and a percent accuracy of 72.13. Semi empirically defined coefficient β was used for the fifteen plots and displays RMSE of 50.17 (t ha⁻¹) and a percent accuracy of 78.6%. Remaining 34 plots were utilized for estimated AGB and showed RMSE of 58.8 (t ha⁻¹) and percent accuracy of 69.09%. In the regression analysis conducted by Chandola (Chandola, 2014) between modelled biomass and field biomass, the coefficient of determination came out to be 0.496. In the present study, the coefficient of determination between modelled biomass and field biomass was 0.47. The variations in the results may be due to the difference in the season of the dataset used. In a work by Poolla (Poolla, 2013) the value of coefficient of determination was 0.431 whereas, in the current study R² was 0.47 between modelled biomass and field biomass. The difference in the values could be because of different wavelength data used i.e. L-band data used by Poolla (Poolla, 2013) and C-band in current work although the modelling approach used is same i.e. EWCM. The other reason is that present study uses the two co-registered images i.e. PolInSAR image.

8. CONCLUSIONS AND RECOMMENDATIONS

8.1. CONCLUSION

This section provides the conclusion of the research work done based on the results gathered following the adopted methodology. The key objective is use of PolInSAR based scattering retrieval for semi-empirical modelling of forest aboveground biomass. All the research objectives were successfully completed in this study. EWCM is utilized for the estimation of biomass. Polarization orientation angle shift compensation was implemented on PolInSAR pair image. PolInSAR pair image was decomposed for the retrieval of different scattering information utilizing a polarimetric Yamaguchi decomposition model. The research questions are as under:

- How to generate PolInSAR based coherency matrix for decomposition?

Combination of co-registered master and slave images were used to generate PolInSAR based coherency matrix. The Pauli feature vector was obtained from master image which was then multiplied by transpose of complex conjugate of slave image. This resulted in generation of PolInSAR based coherency matrix based on equation 4.6.

- How to evaluate the potential of PolInSAR based decomposition modelling for scattering information retrieval?

PolInSAR based coherency matrix was generated over which Yamaguchi decomposition modelling was applied to retrieve scattering information. In this modelling four components, namely, surface scattering, double bounce scattering, volume scattering and helix scattering were retrieved for the estimation of biomass. Volume scattering of PolInSAR image have shown an increasing trend with the increase in field biomass. Surface scattering and double bounce scattering does not show any particular pattern with respect to field AGB for before and after de-orientation.

- What parameters are required to model forest AGB?

For the estimated biomass some parameters are required in EWCM, namely, ground stem backscatter (σ_{gs}^0), back scatter of ground (σ_{gr}^0), backscatter from vegetation (σ_{veg}^0), total forest backscatter (σ_{for}^0) and empirically defined coefficient (β).

- How can PolInSAR based modelling can be used to estimate AGB?

For the estimation of AGB, fifteen plots out of forty nine field plots were used to define the empirically defined coefficient (β) and remaining thirty plots were used to estimate biomass (B). For the fifteen plots, correlation between field biomass (X axis) and modelled biomass (Y axis) was shown to be ($R^2=0.5299$), remaining thirty four plots show the correlation between field biomass (X axis) and modelled biomass (Y axis) as ($R^2=0.43$) and total Fourty nine plots show correlation between field biomass (X axis) and modelled biomass (Y axis) as ($R^2=0.47$).

- What is the accuracy of PolInSAR based semi-empirical model for the accuracy of modelled AGB using field data?

In the PolInSAR image, before-deorientation volume scattering show coefficient of determination as 0.5854 and after-deorientation volume scattering show coefficient of determination as 0.5575. To minimize the overestimation of volume scattering, de-oriented PolInSAR image was used. For Barkot forest zone, modelled biomass show RMSE as 55.18 ($t\ ha^{-1}$) and the accuracy was achieved to be 72%, which relate positively with the field data.

8.2. RECOMMENDATION

In this study PolInSAR based scattering information was retrieved using EWCM using Yamaguchi four decomposition model and the field data. Fully polarimetric Radarsat-2, C band data was used in this study. A couple of suggestions have been included for future studies to upgrade the unwavering quality of the modelling approach for the estimation of AGB.

- EWCM semi empirical modelling was utilized in this study for the estimation of AGB. It is prescribed that a different semi empirical model and regression modelling can be used in further studies. It might be possible that the regression modelling gives better accuracy for the estimation of AGB.
- This study used only 49 sample plot field data for the estimation of AGB. More sample plots can be used for the better accuracy in further study.
- Fully polarimetric C band Radarsat-2 data were used in this study. Further study is recommended using different data sets in L-band and P-band, it can give better results for the assessment of AGB.
- The present research focuses on Barkot forest, which is a homogenous forest. Most of the Sal species are there in this area. 57 percent of Sal species are covered this area. It is recommended that use of present methodology can be applied in heterogeneous forest also which can aid in evaluation of all forest types in the area.
- Incorporation of extra parameters like the impact of soils and stem moisture might further upgrade the understanding and exactness of biomass estimation.

LIST OF REFERENCES

- Amrutkar, R.P., Kumar, S., Kushuwaha, S.P.S., Bhatt, G.D., 2012. Forest biophysical parameter retrieval using polsar technique, in: 8th International Conference on Microwaves, Antenna, Propagation & Remote Sensing-ICMARS, Jodhpur, India.
- Askne, J., Dammert, P.B.G., Israelsson, H., Ulander, L.M.H., 1995. Retrieval of forest parameter using intensity and repeat pass interferometric SAR information. proceeding of Retrieval of Bio- and geophysical Parameter from SAR Data for Land Application, Toulouse.
- Attema, E.P.W., Ulaby, F.T., 1978. Vegetation modeled as a water cloud. *Radio Science* 13, 357–364. doi:10.1029/RS013i002p00357
- Ballester-Berman, J.D., Lopez-Sanchez, J.M., 2010. Applying the Freeman-Durden Decomposition Concept to Polarimetric SAR Interferometry. *IEEE Transactions on Geoscience Remote Sensing* 48, 466–479. doi:10.1109/TGRS.2009.2024304
- Ballester-Berman, J.D., Lopez-Sanchez, J.M., Fortuny-Guasch, J., 2005. Retrieval of biophysical parameters of agricultural crops using polarimetric SAR interferometry. *IEEE Transactions on Geoscience Remote Sensing* 43, 683–694. doi:10.1109/TGRS.2005.843958
- Brown, S., 1997. Estimating biomass and biomass change of tropical forests: a primer. Food & Agriculture Organization, Rome.
- Carreiras, J., Melo, J., Vasconcelos, M., 2013. Estimating the Above-Ground Biomass in Miombo Savanna Woodlands (Mozambique, East Africa) Using L-Band Synthetic Aperture Radar Data. *Remote Sens.* 5, 1524–1548. doi:10.3390/rs5041524
- Chandola, S., 2014. Polarimetric SAR Interferometry for Forest Aboveground Biomass Estimation. M.Sc. Thesis Faculty of Geo-information Science and Earth Observation (ITC) of the University of Twente, Enschede, The Netherlands.
- Chaturvedi, A.N., Khanna, L.S., 1994. Forest Mensuration & Biometry. International Book Distributors.
- Chen, S.-W., Wang, X.-S., Sato, M., 2012. PolInSAR Complex Coherence Estimation Based on Covariance Matrix Similarity Test. *IEEE Transactions on Geoscience Remote Sensing* 50, 4699–4710. doi:10.1109/TGRS.2012.2192937
- Chowdhury, T., Thiel, C., Schmullius, C., Stelmaszczuk-Górska, M., 2013. Polarimetric Parameters for Growing Stock Volume Estimation Using ALOS PALSAR L-Band Data over Siberian Forests. *Remote Sensing* 5, 5725–5756. doi:10.3390/rs5115725
- Cloude, S.R., 2008. POL-InSAR training course. Tutorial ESA Polarimetric SAR Processing PolSARPro Toolbox. http://earth.esa.int/polsarpro/Manuals/1_Pol-InSAR_Training_Course.pdf. (accessed 2014-09-26 01:52:29)
- Cloude, S.R., Papathanassiou, K.P., 2003. Three-stage inversion process for Polarimetric SAR Interferometry. *IEEE Transactions on Geoscience Remote Sensing* 150. doi:IO. 1049/ip-rsn:20030449

- Cloude, S.R., Papathanassiou, K.P., 1998. Polarimetric SAR interferometry. *IEEE Transactions on Geoscience Remote Sensing* 36, 1551–1565. <http://dx.doi.org/10.1109/36.718859>.
- Cloude, S.R., Pottier, E., 1996. A review of target decomposition theorems in radar polarimetry. *IEEE Transactions on Geoscience Remote Sensing* 34, 498–518. doi:10.1109/36.485127
- Colin-Koeniguer, E., Trouve, N., 2014. Performance of Building Height Estimation Using High-Resolution PolInSAR Images. *IEEE Transactions on Geoscience Remote Sensing* 52, 5870–5879. doi:10.1109/TGRS.2013.2293605
- Ding, C.-S., Wu, Q., Ta Hsieh, C., M., P., 1998. Stratified random sampling for power estimation, in: *In Proceedings of the 1996 IEEE/ACM International Conference on Computer-Aided Design*. California, pp. 465 – 471. doi:10.1109/43.703828
- Dinh, H.T.M., Rocca, F., Tebaldini, S., d' Alessandro, M.M., Le Toan, T., Villard, L., 2012. Relating tropical forest biomass to P-band SAR tomography, in: *Geoscience and Remote Sensing Symposium (IGARSS), 2012 IEEE International*. IEEE, pp. 7589–7592.
- Food and Agriculture Organization of the United Nations, 2012. State of the world's forests, 2012. FAO report, United Nations, Rome.
- Food and Agriculture Organization of the United Nations, 2004. Global forest resources assessment update 2005 terms and definitions. Food and Agriculture Organization of the United Nations, Rome, Italy.
- Forest Survey of India, 1996. Volume Equation for Forests of India, Nepal and Bhutan. Ministry of Environment and Forests, Dehradun, India.
- Freeman, A., Durden, S.L., 1998. A three-component scattering model for polarimetric SAR data. *IEEE Transactions on Geoscience Remote Sensing* 36, 963–973.
- HariPriya, G.S., 2002. Biomass carbon of truncated diameter classes in Indian forests. *Forest Ecology and Management* 168, 1–13.
- Hellmann, M., Cloude, S.R., 2005. Polarimetric interferometry and differential interferometry. Adelaide University School of Electrical and Electronic Engineering, Australia.
- Henderson, F.M., Lewis, A.J., 1998. Principles and Applications of Imaging Radar: Manual of remote sensing. John Wiley and sons, New York.
- Huang, Y., Qiaoping, Z., Marcus, S., Ming, W., 2014. Biomass Estimation of Boreal Forests Using Single-Pass Polarimetric SAR Tomography at L-band. Presented at the EUSAR 2014; 10th European Conference on Synthetic Aperture Radar, VDE, Germany, pp. 1 – 4.
- Husch, B., Beers, T.W., Kershaw, J.A., 2003. Forest mensuration, 4th ed. John Wiley & Sons, New Jersey.
- Huyen, J.R., 1970. Phenomenological theory of radar targets, PhD thesis. Technical University, Delft, Netherlands.
- Imhoff, M.L., 1995. Radar backscatter and biomass saturation: ramifications for global biomass inventory. *IEEE Transactions on Geoscience Remote Sensing* 33, 511–518.
- Iribe, K., Sato, M., 2007. Analysis of Polarization Orientation Angle Shifts by Artificial Structures. *IEEE Transactions on Geoscience Remote Sensing* 45, 3417–3425. doi:10.1109/TGRS.2007.905973

- Jahan, S., Ahmed, I., 2010. Operation properties of Adjoint Matrix of Hermitian Block Matrices. *International Journal of Basic Applied Science* 10.
- Jin, Y.-Q., Feng, X., 2013. *Polarimetric scattering and SAR information retrieval*. John Wiley & Sons, Singapore.
- Kimura, H., 2008. Radar Polarization Orientation Shifts in Built-Up Areas. *IEEE Transactions on Geoscience Remote Sensing Letters* 5, 217–221. doi:10.1109/LGRS.2008.915737
- Kirilenko, A.P., Sedjo, R.A., 2007. Climate change impacts on forestry. *Proceedings of the National Academy of Science* 104, 19697–19702. doi:10.1073/pnas.0701424104
- Kumar, S., 2009. Retrieval of forest parameters from Envisat ASAR data for biomass inventory in Dudhwa National Park, U.P., India. Faculty of Geo-information Science and Earth Observation (ITC) of the University of Twente, Enschede, The Netherlands.
- Kumar, S., Pandey, U., Kushwaha, S.P., Chatterjee, R.S., Bijker, W., 2012. Aboveground biomass estimation of tropical forest from Envisat advanced synthetic aperture radar data using modeling approach. *Journal of Applied Remote Sensing* 6, 063588–063588.
- Lamei Zhang, Bin Zou, Hongjun Cai, Ye Zhang, 2008. Multiple-Component Scattering Model for Polarimetric SAR Image Decomposition. *IEEE Transactions on Geoscience Remote Sensing Letters* 5, 603–607. doi:10.1109/LGRS.2008.2000795
- Lavalle, M., Solimini, D., Pottier, E., Desnos, Y.-L., 2008. PolinSAR for forest biomass retrieval: PALSAR observations and model analysis, in: *Geoscience and Remote Sensing Symposium, 2008. IGARSS 2008*. IEEE International. IEEE, pp. III–302.
- Lee, J.-S., Ainsworth, T.L., 2011. The Effect of Orientation Angle Compensation on Coherency Matrix and Polarimetric Target Decompositions. *IEEE Transactions on Geoscience Remote Sensing* 49, 53–64. doi:10.1109/TGRS.2010.2048333
- Lee, J.-S., Pottier, E., 2009. *Polarimetric Radar Imaging: From Basics to Applications*. CRC Press, Florida.
- Lee, J.-S., Schuler, D.L., Ainsworth, T.L., 2003. A review of polarization orientation estimation from polarimetric SAR data, in: *Applications of SAR Polarimetry and Polarimetric Interferometry*. p. 3.
- Lee, J.S., Schuler, D.L., Ainsworth, T.L., Boerner, W.M., 1999. POLSAR data compensation for terrain azimuth slope variation, in: *Geoscience and Remote Sensing Symposium, 1999. IGARSS'99 Proceedings*. IEEE 1999 International. IEEE, pp. 2437–2439.
- Le Toan, T., Ulander, L., Papathanassiou, K., Villard, L., Scipal, K., 2014. Biomass retrieval from P-band polarimetric and interferometric SAR data, challenges and recent results, in: *Geoscience and Remote Sensing Symposium (IGARSS), 2014 IEEE International*. IEEE, pp. 1417–1420.
- Limaye, V.D., Sen, B.R., 1956. *Weight and Specific Gravity of Indian Woods*. Forest Research Institute, Indian Forest Records, Dehradun, India.
- Lin, Y.-C., Sarabandi, K., 1998. Tree parameter estimation from interferometric radar responses, in: *Geoscience and Remote Sensing Symposium Proceedings, 1998. IGARSS'98*. 1998 IEEE International. IEEE, pp. 2436–2438.

- Li, Z., Bethel, J., 2008. Image coregistration in SAR interferometry. *Proc Int Arch Photogramm Remote Sens Spat. Inf Sci* 433–438.
- Lopez-Sanchez, J.M., Hajnsek, I., Ballester-Berman, J.D., 2012. First Demonstration of Agriculture Height Retrieval With PolInSAR Airborne Data. *IEEE Transactions on Geoscience Remote Sensing Letters* 9, 242–246. doi:10.1109/LGRS.2011.2165272
- Lumsdon, P., Mercer, B., Zhang, Q., 2008. Estimation and Monitoring of Tropical Forest Biomass Using Polarimetric Interferometric SAR Data. *Intermap Technol. Corp.*
- Main-Knorn, M., Moisen, G.G., Healey, S.P., Keeton, W.S., Freeman, E.A., Hostert, P., 2011. Evaluating the Remote Sensing and Inventory-Based Estimation of Biomass in the Western Carpathians. *Remote Sens.* 3, 1427–1446. doi:10.3390/rs3071427
- Mette, T., Papathanassiou, K., Hajnsek, I., 2004. Biomass estimation from polarimetric SAR interferometry over heterogeneous forest terrain, in: *Geoscience and Remote Sensing Symposium, 2004. IGARSS'04. Proceedings. 2004 IEEE International. IEEE*, pp. 511–514.
- Mette, T., Papathanassiou, K.P., Hajnsek, I., Zimmermann, R., 2002. Forest biomass estimation using polarimetric SAR interferometry. Presented at the *Geoscience and Remote Sensing Symposium, 2002. IGARSS '02. 2002 IEEE International, IEEE, Toronto, Canada*, pp. 817 – 819. doi:10.1109/IGARSS.2002.1025695
- Minh, N.P., Zou, B., Lu, D., 2012. Accuracy improvement method of forest height estimation for PolInSAR Image, in: *Audio, Language and Image Processing (ICALIP), 2012 International Conference on. IEEE*, pp. 594–598.
- Neumann, M., Ferro-Famil, L., Reigber, A., 2010. Estimation of Forest Structure, Ground, and Canopy Layer Characteristics From Multibaseline Polarimetric Interferometric SAR Data. *IEEE Trans. Geosci. Remote Sens.* 48, 1086–1104. doi:10.1109/TGRS.2009.2031101
- Neumann, M., Saatchi, S.S., Ulander, L.M., Fransson, J.E., 2011. Parametric and non-parametric forest biomass estimation from PolInSAR data, in: *Geoscience and Remote Sensing Symposium (IGARSS), 2011 IEEE International. IEEE*, pp. 420–423.
- Papathanassiou, K.P., Cloude, S.R., 2001. Single-baseline polarimetric SAR interferometry. *Geosci. Remote Sens. IEEE Trans. On* 39, 2352–2363.
- Poolla, S. bharadwaj, 2013. Polarimetric scattering model for biophysical characterization of multilayer vegetation using space borne PolSAR data. M.Sc. Thesis Faculty of Geo-information Science and Earth Observation (ITC) of the University of Twente, Enschede, The Netherlands.
- Praks, J., Kugler, F., Papathanassiou, K.P., Hajnsek, I., Hallikainen, M., 2007. Height Estimation of Boreal Forest: Interferometric Model-Based Inversion at L- and X-Band Versus HUTSCAT Profiling Scatterometer. *IEEE Transactions on Geoscience Remote Sensing Letters* 4, 466–470. doi:10.1109/LGRS.2007.898083
- Rahman, M.M., Tetuko Sri Sumantyo, J., 2013. Retrieval of tropical forest biomass information from ALOS PALSAR data. *Geocarto Int.* 28, 382–403. doi:10.1080/10106049.2012.710652
- Santoro, M., 2003. Estimation of biophysical parameters in boreal forests from ERS and JERS SAR interferometry. Ph. D Thesis Department of Radio and Space Science, Chalmers University of Technology.

- Santoro, M., Askne, J., Eriksson, L., Schmullius, C.C., Wiesmann, A., Fransson, J., 2003. Seasonal dynamics and stem volume retrieval in boreal forests using JERS-1 backscatter, in: International Symposium on Remote Sensing. International Society for Optics and Photonics, pp. 231–242.
- Santoro, M., Eriksson, L., Askne, J., Schmullius, C., 2006. Assessment of stand-wise stem volume retrieval in boreal forest from JERS-1 L-band SAR backscatter. *International Journal of Remote Sensing* 27, 3425–3454. doi:10.1080/01431160600646037
- Touzi, R., 2007. Target Scattering Decomposition in Terms of Roll-Invariant Target Parameters. *IEEE Transactions on Geoscience Remote Sensing* 45, 73–84. doi:10.1109/TGRS.2006.886176
- Touzi, R., Boerner, W.M., Lee, J.S., Lueneburg, E., 2004. A review of polarimetry in the context of synthetic aperture radar: concepts and information extraction. *Canadian Journal of Remote Sensing* 30, 380–407.
- Wollersheim, M., Collins, M.J., 2008. Extraction of Forest Biophysical Parameters Using Polarimetric SAR, in: Geoscience and Remote Sensing Symposium, 2008. IGARSS 2008. IEEE International. IEEE, pp. II–625.
- Woodhouse, I.H., 2006. Introduction to microwave remote sensing. Taylor & Francis, Boca Raton.
- Yamaguchi, Y., Moriyama, T., Ishido, M., Yamada, H., 2005. Four-component scattering model for polarimetric SAR image decomposition. *IEEE Transactions on Geoscience Remote Sensing* 43, 1699–1706. doi:10.1109/TGRS.2005.852084
- Yamaguchi, Y., Sato, A., Boerner, W.-M., Sato, R., Yamada, H., 2011. Four-Component Scattering Power Decomposition With Rotation of Coherency Matrix. *IEEE Transactions on Geoscience Remote Sensing* 49, 2251–2258. doi:10.1109/TGRS.2010.2099124
- Zianis, D., Suomen Metsätieteellinen Seura, Metsätutkimuslaitos (Eds.), 2005. Biomass and stem volume equations for tree species in Europe, *Silva Fennica monographs*. Finnish Society of Forest Science, Finnish Forest Research Institute, Helsinki, Finland.

APPENDIX: DECOMPOSITION IMAGE OF RADARSAT-2 DATA

Yamaguchi decomposition of Radarsat-2 data for Barkot Forest range (Master image- RGB image)

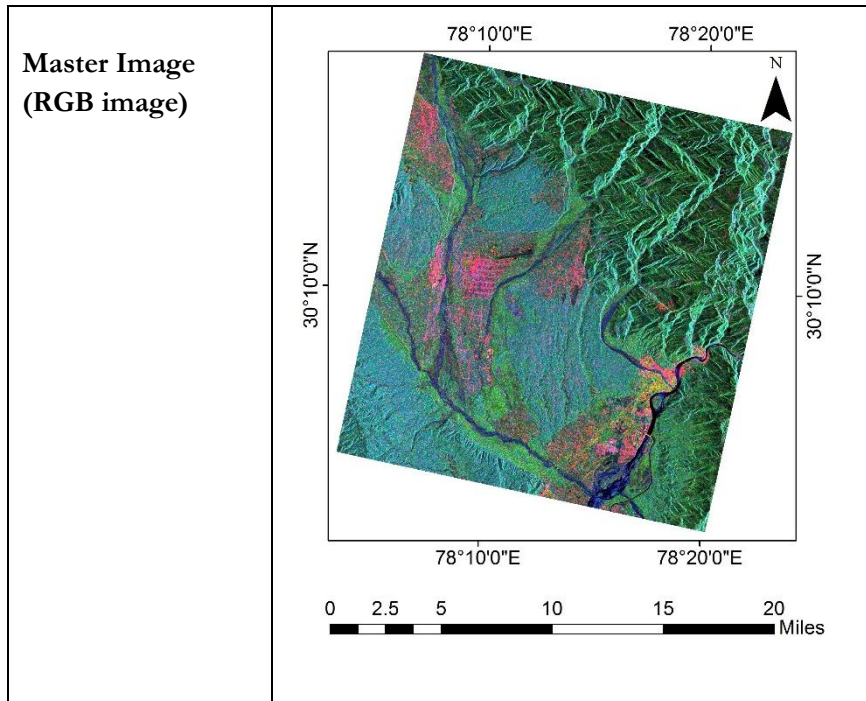


Figure A: Yamaguchi decomposition of master image

Yamaguchi decomposition of Radarsat-2 data for Barkot Forest range (Slave image – RGB image)

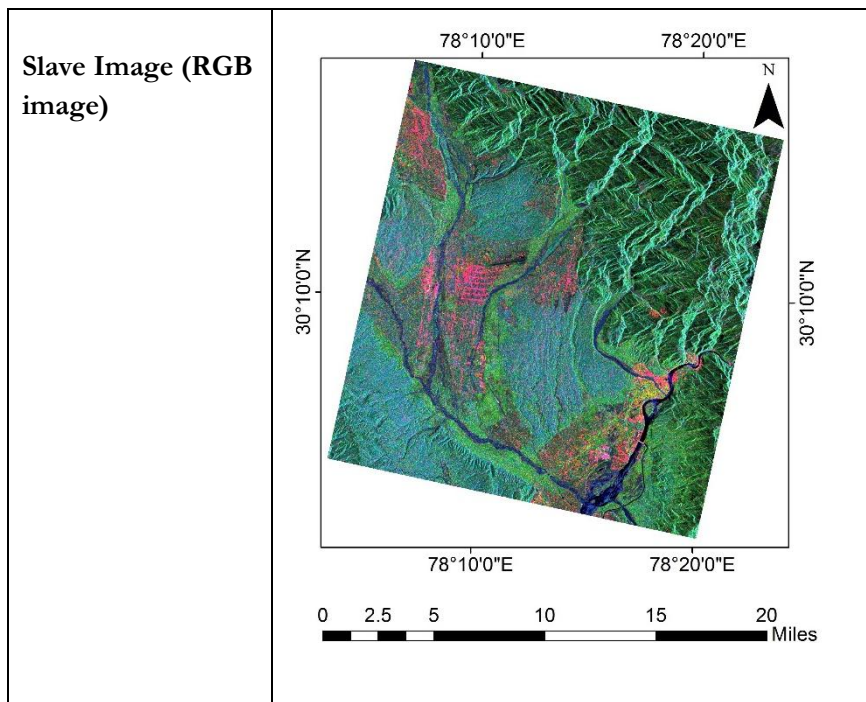


Figure B: Yamaguchi decomposition of slave image